BRNO UNIVERSITY OF TECHNOLOGY

VYSOKÉ UČENÍ TECHNICKÉ V BRNĚ

FACULTY OF MECHANICAL ENGINEERING

FAKULTA STROJNÍHO INŽENÝRSTVÍ

INSTITUTE OF PHYSICAL ENGINEERING

ÚSTAV FYZIKÁLNÍHO INŽENÝRSTVÍ

METHODS FOR DETECTING THE FREQUENCY OF CENTERS OF HYDROGEN-CYANINE (HCN) HYPERFINE TRANSITIONS USING A TUNABLE LASER IN THE RANGE 1527 NM TO 1563 NM

METODY DETEKCE FREKVENCE STŘEDŮ HYPERJEMNÝCH ABSORPČNÍCH ČAR KYANOVODÍKU (HCN) POMOCÍ PŘELADITELNÉHO LASERU V ROZSAHU 1527 NM AŽ 1563 NM

DOCTORAL THESIS SUMMARY

TEZE DIZERTAČNÍ PRÁCE

AUTHOR
AUTOR PRÁCE

Ing. Martin Hošek

SUPERVISOR
ŠKOLITEL

Ing. Ondřej Číp, Ph.D.

BRNO 2024

Abstrakt
Kyanovodík (HCN) je médiem, jehož absorpční spektrum pokrývá celé telekomunikační C-pásmo. To dělá z HCN vhodného kandidáta pro použití při frekvenční stabilizaci laserů. Tato práce se zaměřuje na přesné měření středů absorpčních čar HCN, což povede k zvýšení užitečnosti tohoto plynu v praxi. Cíle práce je dosaženo pomocí dvou metod laserové spektroskopie, a to lineární absorpční spektroskopie a saturované absorpční spektroskopie. Je sestavena tabulka absorpčních čar HCN, kde nejistota frekvence středů čar dosahuje čtyřicetinásobného zlepšení oproti doposud neměřené nejistotě.

Summary
Hydrogen cyanide (HCN) is a medium whose absorption spectrum covers the whole telecommunication C-band. This makes HCN a great candidate to use in laser frequency locking. The focus of the thesis is the precise measurement of the HCN absorption lines' centres frequency, improving the usefulness of the gas for the applications. This goal is achieved by utilising two laser spectroscopy techniques: linear absorption spectroscopy and saturation absorption spectroscopy. The table of HCN absorption lines was built, with the uncertainty of their central frequency being about fortyfold better than the state-of-art uncertainty.

Klíčová slova
laserová spetroskopie, lineární absorpční specktroskopie, saturovaná absorpční spektroskopie, kyanovodík, frekvenčně stabilizované lasery

Keywords
laser spectroscopy, linear absorption spectroscopy, saturation absorption spectroscopy, hydrogen cyanide, frequency stabilised lasers

HOSEK, M.*Methods for detecting the frequency of centers of Hydrogen-Cyanine (HCN) hyperfine transitions using a tunable laser in the range 1527 nm to 1563 nm.* Brno: Vysoké učení technické v Brně, Fakulta strojního inženýrství, 2024. 37 s. Vedoucí Ing. Ondřej Číp, Ph.D.

Contents

1. Introduction and structure of the work

The current definition of the meter is: "The metre, symbol m, is the SI unit of length. It is defined by taking the fixed numerical value of the speed of light in vacuum c to be 299 792 458 when expressed in the unit $\mathrm{m} \cdot \mathrm{s}^{-1}$, where the second is defined in terms of the caesium frequency $\Delta\nu_{Cs}$" [1]. "

In practice, not every laboratory or industrial company can have such experimental devices to realise the unit according to its definition. For this purpose, the International Bureau of Weights and Measures (BIPM from *Bureau International des Poids et Mesures*) publishes the Mise en Pratique, giving the recommended approach to realise a particular unit with the given uncertainty.

Regarding one meter [2], frequency-locking the laser to the minimum of a specific absorption line is a valuable way of realising it. A laser of this kind possesses a very stable frequency or wavelength with the unit of 1 m, which can also be transferred to the period of oscillation with the unit of 1 s. The list of such suitable absorption lines is called the "Recommended values of standard frequencies" [3].

In the visible part of the spectrum, the list of "Recommended values of standard frequencies" includes eight iodine absorption lines. This makes iodine the cornerstone in frequency metrology and associated laser spectroscopy [4], [5], [6]. On the other hand, in the near-infrared spectrum, the only absorption line presented on the list is P16 ($\nu_1 + \nu_3$) band of acetylene $^{13}C_2H_2$. The central frequency of this line is known with the uncertainty of 1 kHz. As the accessibility of isotopically pure acetylene is getting limited, the demand for alternative absorption medium in the near-infrared spectrum is increasing.

$H^{13}C^{14}N$ is an absorption medium with an advantage over acetylene, having a wider absorption spectrum Fig. 1.1. The absorption spectrum of hydrogen cyanide covers well the telecommunication C-band (1530 - 1560 nm), making it the ideal candidate for use in optical fibre communication. The absorption lines of $H^{13}C^{14}N$ were studied in the past (more on this is reviewed in Chapter 5). Due to the use of not-so-precise techniques, the positions of line centres are known a thousand times less precisely than those of $^{13}C_2H_2$. Moreover, the authors in [7] observe discrepancies in results using $H^{13}C^{14}N$ for laser frequency stabilisation in frequency scanning interferometry (FSI).

The $H^{13}C^{14}N$ absorption lines measurement became one of the work packages of the Large Volume Metrology Applications (LaVA) project (funded by EC/EURAMET, project number l EMPIR 17IND03). The project consortium included leading European National Metrology Institutes (e.g. National Physical Laboratory (NPL) from the United Kingdom, National Metrology Institute of Italy (INRIM from *L'Istituto Nazionale di Ricerca Metrologica*) and National Laboratory of Metrology and Testing (LNE from *Laboratoire national de métrologie et d'essais*) from France), their research partners (e.g. the Institute of Scientific Instruments (ISI from *Ústav přístrojové techniky*) from the Czech Republic and the National Conservatory of Arts and Crafts (CNAM from *Conservatoire national des arts et métiers*) from France) and industrial partners (e.g. SAAB AKTIEBOLAG from Sweden, Oy Mapvision from Finland).

Structure of the work: Chapter 2 describes the goals of the thesis that are to be met. The objectives are structured in five points. Together with a brief explanation, they provide crucial insights on the content and focus of the thesis' experimental path.

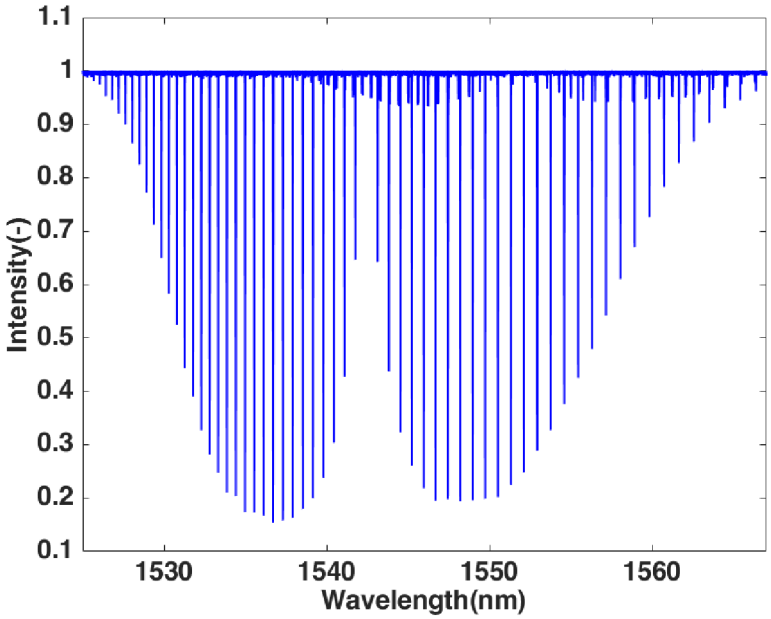

Figure 1.1: Absorption spectrum of $H^{13}C^{14}N$ $2\nu_3$ absorption band.

The major themes of the Chapter 3 are the highly-tunable laser sources and optical frequency combs. The principle of laser and optical frequency comb is described there, and particular lasers used in the experimental part of the thesis are mentioned too.

In this work, two laser spectroscopy methods are used: specifically the linear absorption spectroscopy and the saturation absorption spectroscopy. Both methods are explained in the Chapter 4. The principle of the methods and the limitations of their use are included in this chapter.

The current state of scientific knowledge in measurement of $H^{13}C^{14}N$ absorption lines is the topic of Chapter 5. The chapter is focusing on the analysis of the most up-to-date articles as well as the assessment of the measured results.

In Chapter 6, the linear spectroscopy experiments are explained. The results obtained using the experimental setups are shown. Furthermore, their precision and accuracy are commented on.

The Chapter 7 is focusing on the saturation absorption spectroscopy. The gradual progress described in this chapter led to the publication of the article [8], that is also analysed in this chapter.

2. Thesis objectives

The objectives of my thesis can be summarised in several points (see below). Those are heading towards the ultimate goal of writing down the table of $H^{13}C^{14}N$ absorption lines centre in the $2\nu_3$ band with corresponding optical frequencies. The new table will be helpful for many areas, especially for the metrology of length.

1. **Select a laser source allowing fast tuning of the optical frequency with narrow linewidth of the spectral line.**

   The spectrum of $H^{13}C^{14}N$ covers range from from 1527 nm to 1563 nm, which is approx. 36 nm. It is one of the advantages of $H^{13}C^{14}N$ as an absorption medium over the conventionally used C_2H_2. At the same time it is also necessary to find a laser, that allows to scan over the whole spectrum within reasonable timeframe without any optical frequency mode-hops. The important objective is to acquire such a laser and get familiar with controlling it.

2. **Design and implement the experimental equipment to realise the linear absorption spectroscopy with laser optical frequency traceable to optical frequency comb.**

   The linear absorption spectroscopy, as described in section 4.1, is a relatively simple method which allows the measurement of absorption lines centre. The authors in [9] used to measure $H^{13}C^{14}N$ absorption lines with the uncertainty of about 1 MHz. The improvement of the laser optical frequency precision by using the optical frequency comb will lead to a better evaluation of frequencies of $H^{13}C^{14}N$ spectral line centres.

3. **Design and set up a modulation-free saturation absorption spectroscopy method and develop a vacuum apparatus for a low-pressure spectroscopy of $H^{13}C^{14}N$ gas.**

   The saturation absorption spectroscopy is a method allowing for Doppler-free spectroscopical measurement. Compared to the linear absorption spectroscopy, it enables about three orders of magnitude more precise absorption lines centre determination. On the other hand, it is a more sophisticated method. It has been used for $H^{13}C^{14}N$ measurement in the past, as discussed in the section 5.2, but no systematical measurement of absorption lines position has been performed so far. Besides, it was also necessary to develop a vacuum apparatus for filling the cell with $H^{13}C^{14}N$ gas allowing for precise control of the $H^{13}C^{14}N$ gas pressure.

4. **Measure precisely the optical frequency of hyperfine line centres of $H^{13}C^{14}N$.**

   The knowledge of $H^{13}C^{14}N$ absorption lines centre is helpful not only from the fundamental research point of view. In the frequency scanning interferometry, the uncertainty u_{f1}, u_{f2} of the centre's frequency f_1, f_2 has a direct impact on the uncertainty of length measurement u_c. These uncertainties relate as $u_c = (u_{f1} - u_{f2})/(f_1 - f_2)$. Further improvement of $H^{13}C^{14}N$ data can have a positive impact on this method's precision.

5. **Assemble the resultant table of optical frequencies of the measurement of the individual hyperfine $H^{13}C^{14}N$ transition centres in the band from**

1527 nm **to** 1563 nm**. Compare that table with the data obtained in the past by less accurate linear absorption spectroscopy.**

The precise measurement of the $H^{13}C^{14}N$ absorption lines centre has the potential to establish $H^{13}C^{14}N$ on the list of *Recommended values of standard frequencies* [3] and be included in *Mise en pratique for the definition of the metre in the SI* [10].

3. Highly-coherent tunable laser sources and optical frequency combs

The first optical maser or laser (Light Amplification by Stimulated Emission of Radiation) was constructed in 1960 by T.H. Mainman. C. H. Townes, N. Basov, and A. Prokhorov shared the Nobel Prize in Physics *for fundamental work in the field of quantum electronics, which has led to the construction of oscillators and amplifiers based on the maser–laser principle* [11] in 1964.

Assuming, to simplify, the two energy levels model. In the case of radiation, with energy corresponding to the difference in energy levels, three processes occur. The electrons in the lower energy level can absorb the radiation and they can be excited to the higher energy level. This process is called induced absorption. Meanwhile, the electrons in the higher absorption level can deexcite to the lower energy level and convert their excitation energy to photons.

The third process, enabled by the radiation, is stimulated emission. As the electrons on the higher energy level "sense" the presence of the radiation field, they can deexcite to the lower energy level. The excitation energy transforms into photons with precisely the same phase, polarisation and direction of propagation as the photons in the presented radiation field.

As the absorption and the emission effects occur simultaneously, conditions for the emission dominating the absorption need to be established. It means that the number of electrons in the higher energy level has to prevail over those in the lower energy level. The so-called population inversion can be achieved in several ways, e.g. external laser pumping and arc lamp pumping.

3.1. Lasers used in the experimental setups

In the experiments described in this thesis, two lasers were mostly used. Koheras Adjustik E15 and CTL 1550. The main features of both of them are described in the upcoming sections.

3.1.1. Koheras Adjustik E15

In the preliminary experiments, applying to both linear absorption spectroscopy and saturation absorption spectroscopy, the Koheras Adjustik E15 was used. It is a DFB (distributed feedback) fibre laser allowing the laser frequency scan in the range from $\approx$1539.8 nm to $\approx$1541.0 nm. The laser frequency can be tuned by changing the laser diode temperature or the piezo crystal voltage. Moreover, the piezo crystal allows for laser frequency modulation up to 20 kHz with the modulation width up to 8 GHz. The frequency linewidth of the laser is below 0.1 kHz, and the maximum optical output power is 40 mW. The laser is controllable through USB and ethernet interfaces.

The Koheras Adjustik E15 allows to measure one $H^{13}C^{14}N$ absorption line. At the same time, it was the ideal solution for the preliminary measurement thanks to its

availability and accessibility at the Institute of Scientific Instruments (ISI) of the Czech Academy of Sciences (where the experimental part of my studies took place).

In the latter experiments, the CTL 1550 laser was used. Utilising the CTL 1550 allowed to measure the whole absorption spectrum of $H^{13}C^{14}N$.

3.1.2. CTL 1550

Continuously-tunable laser (CTL 1550, TOPTICA Photonics AG) is an external cavity semiconductor laser (ECSL) with a tuning range from 1510 nm to 1630 nm. The wide frequency (wavelength) scan is enabled by motor. It allows to scan with the speed up to 10 nm/s. The fine tuning can be performed by a piezo actuator with the range of 35 GHz and a resolution of a few kHz.

The laser current can be modulated using a DC input with the bandwidth limit at 100 MHz, the sensitivity of 0.73 mA/V and an input range ±5 V. The alternative for laser current modulation is an AC input, which allows a modulation above 100 kHz. The sensitivity of the input is 2.2 mA/V with the input range of ±1.8 V.

The laser has an integrated isolator and the FiberDock collimator with a focal length of 11 mm. The maximum optical output power behind the fibre collimator is 39 mW. The frequency linewidth of the laser beam is bellow 10 kHz.

The mode-hope free operation of the CTL is ensured by synchronous tuning of all of the frequency-sensitive elements. It is guaranteed by SMILE (Single Mode Intelligent Loop engine). The communication with the laser can be facilitated in multiple ways, either using a DLC pro controller, USB, or Ethernet interface.

3.2. Optical frequency comb

An optical frequency comb (OFC) is a unique laser device whose frequency spectrum consists of many equally spaced spikes (teeth). As the frequency spectrum of the OFC can cover a significantly broad part of the spectrum (in order of 100 THz), it allows us to compare the stability of lasers at different frequencies. We can observe its influence in many fields, such as a frequency metrology and a distance measurement. It led to the awarding of the Nobel Prize in Physics to J. L. Hall and T. W. Hänsch *for their contributions to the development of laser-based precision spectroscopy, including the optical frequency comb technique* [12] in 2005.

The frequency of the OFC f_n can be expressed as:

$$f_n = nf_r + f_0, \tag{3.1}$$

where n is the integer signing the order of the OFC tooth, f_r is the repetition frequency, and f_0 is the offset frequency. The offset frequency is caused by the offset between the electric field and the pulse envelope (sometimes called carrier envelope offset). To minimise the uncertainty of the f_0, it is stabilised. One of the convenient ways to do so is to suppress the fluctuation of laser cavity length using a piezoelectric crystal.

The repetition rate of the OFC is equal to the inverted value of the pulse repetition rate in the time domain Fig. **??**. The stabilisation of the whole OFC spectrum can be done by stabilisation of f_r and f_0. By doing that, we can get a broad-spectrum device that permits us to compare the stability of the laser source. Another application of OFC

is measuring the precise frequency of the laser by beating it against OFC, as will be discussed later in this work.

4. Laser spectroscopy

A laser spectroscopy includes many methods and techniques for investigating atoms and molecules as well as their characteristics [13]. It can be derived from the absorption or emission spectrum, that provides the information about the atomic structure and the composition of unknown matter. The intensity of the line is proportional to transition probability, which tells how strongly are the two levels of the transitions coupled. All these pieces of information enable to better understand the world around us and to better describe it.

From all of the methods in the laser spectroscopy family, I decided to invest in studying in detail linear absorption spectroscopy and saturation absorption spectroscopy. The first one has the advantage of being relatively simple and, simultaneously, allowing to study the absorption lines with high accuracy [14], [15]. The latter permits overcoming the principal limitation of linear absorption spectroscopy by removing the Doppler broadening.

Worth mentioning is the fact that both methods were deeply studied and used for I_2 absorption lines' measurement [16],[17] at the Institute of Scientific Instruments (ISI) of the Czech Academy of Sciences in the past. Besides, the experimental part of my studies took place at ISI.

4.1. Linear absorption spectroscopy

4.1.1. Principle of the method

In the linear absorption spectroscopy, the laser beam passes through the absorption medium. As the frequency of the laser source is tuned over the absorption line profile, the transmitted optical power is recorded on the photodetector Fig. 4.1. The signal from the photodetector is then combined with the information about laser source frequency. Afterwards, the position of the absorption line centre can be retrieved.

Given that each spectral line absorbs differently, the less it absorbs, the more challenging (less accurate) is the absorption line centre determination. The absorption can be maximised by extending the length of the absorption gas cell, using the multi-pass arrangement or by increasing the gas pressure. While growing pressure in the gas cell leads to the significant pressure broadening of the absorption lines, cell's widening has practical limitations. Another option is to modulate the laser beam frequency [18], [19].

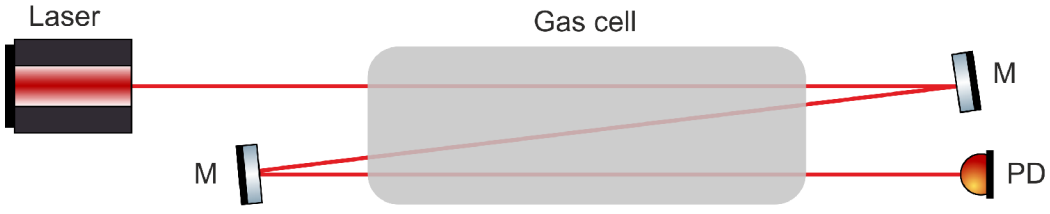

Figure 4.1: Principle of linear absorption spectroscopy: mirrors (M), and photodetector (PD).

4.1.2. Modulation of the laser optical frequency

Laser's optical frequency modulation improves the signal-to-noise (S/N) ratio of the detected absorption signal thanks to the background noise suppression. It allows to cancel the low-frequency noise while detecting the optical signal on higher harmonic frequencies. Modulation of the laser optical frequency has applications not only in laser spectroscopy but also in encoding, telecommunication, and other technical disciplines.

The frequency of the wave, in our case, light f_L, is periodically changed with the amplitude Δf. The resulting frequency f_{modul} can be described as:

$$f_{modul} = f_L + \Delta f \cos \omega t, \tag{4.1}$$

where ω is the angular modulation frequency and t is time.

The enhancement of modulation amplitude improves the S/N ratio of the detected signal. The limit of this effect is different depending on the demodulation frequency, and it increases with the m. For the first harmonic detection, it is 0.7 times half width at half maximum (HWHM) of the absorption line, and for the third harmonic, 1.6 times HWHM. The amplitude of lower harmonic signals generally possesses higher amplitude. The need for lower modulation amplitude, makes them better for practical use. On the other hand, the detection on higher harmonics allows suppressing the residual amplitude modulation.

The modulated signal is subsequently detected on the photodetector and demodulated [21]. The photodetector signal in linear absorption spectroscopy is usually demodulated on the first harmonic frequency. The disadvantage of higher harmonic frequencies demodulation is that it requires higher modulation amplitude to maximise the S/N ratio. Due to Doppler broadened lines, the need for the modulation amplitude is too high, and the negative effects (e.g. residual amplitude modulation (RAM)) would dominate the signal of lower harmonics.

4.1.3. Limitation of the linear absorption spectroscopy

The linear absorption spectroscopy is relatively simple method with all advantages and disadvantages it broughts. The principal limitation is the HWHM of the measured absorption line. I will be dedicating the following lines to the dominant broadening mechanism in linear absorption spectroscopy.

As natural broadening represents the limit of how narrow the absorption line can be, there are many other sources of line broadening (pressure broadening, collisional broadening, transit time broadening, and others). The broadening source can be divided into two groups depending on which absorption line profiles they create, Gauss or Lorentz.

The Doppler broadening is the dominant broadening mechanism of the absorption lines in linear absorption spectroscopy. It is caused by molecules in the gas cell moving randomly. The molecules having the non-zero velocity component in the direction parallel to the laser beam "feel" the laser frequency as different from the actual frequency of the laser source. This makes molecules to absorb the laser radiation on different laser source frequencies, and the absorption lines are broadened. Doppler broadening (having a Gaussian profile) dominant mechanism limiting the accuracy of the linear absorption spectroscopy. Several methods allow Doppler-free measurement [22]. Out of those methods, in my experiments I used the saturation absorption spectroscopy.

The saturation absorption spectroscopy is the content of the following section.

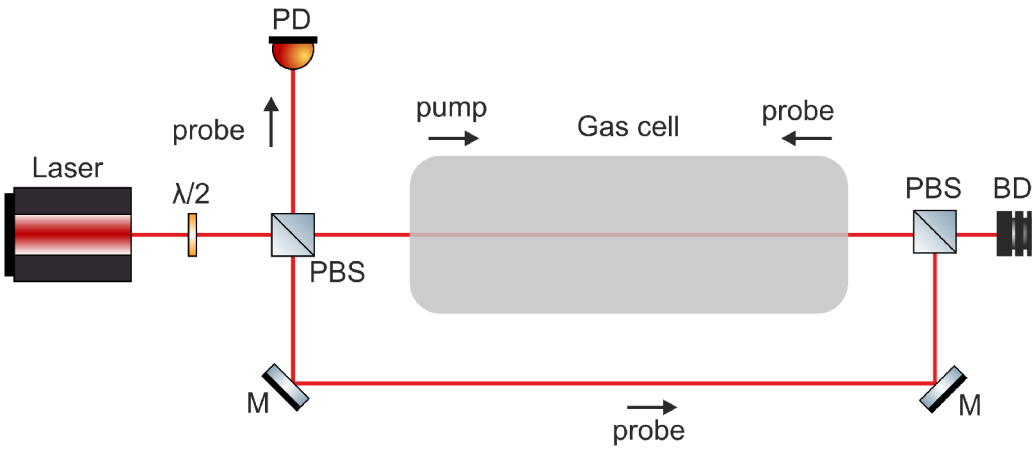

Figure 4.2: Principle of saturation absorption spectroscopy: beam-dump (BD), half-wave plate ($\lambda/2$), mirrors (M), polarising beam splitters (PBS), photodetector (PD).

4.2. Saturation absorption spectroscopy

4.2.1. Principle of the method

Quantitatively, the optical power/intensity needed for the saturation of the absorption line was described in [22]. For sufficiently low I_0, the absorptive coefficient can be assumed as independent of I_0. It means that the intensity of absorbed light is directly proportional to the incoming intensity. As the I_0 increases, this assumption is not valid. It is caused by the insufficient number of electrons in the lower state of the energy transition. If the number of absorbing electrons exceeds the number of electrons getting back by relaxation processes, there are no other electrons left to absorb the incoming light. The transition reaches the saturation, and the absorbed light is no longer directly proportional to the incoming light.

The saturation of the energy transition can be used in the saturation absorption spectroscopy for measuring the Doppler-free absorption lines. The example of the experimental setup Fig. 4.2 consists of two counter-propagating laser beams. The laser beam goes through the half-wave plate, which, in combination with the polarising beams splitter (PBS), allows for the division of the beam power in a variable ratio. The high-power pump beam then transmits through the PBS and the gas cell, and it is absorbed at the beam-dumb. The low-power probe beam is reflected at PBS, then it goes all the way around the gas cell, and after reflecting on the other PBS, it passes through the gas cell in precisely opposite direction than the pump beam. The probe beam measures the line profile saturated by the pump beam, and thus, it is monitored by the photodetector.

The profile of the saturated absorption line Fig. 4.3 has the so-called Lamb dip at the centre, caused by the frequency-selective saturation of molecular transition. The optical power has to be optimised to maximise the depth of the dip.

The saturation coefficient S describes quantitatively the degree of a certain energy transition saturation. The formula for S derived in [22] goes as follows:

$$S = \frac{P}{A}\frac{B_{12}}{cR^*}, \tag{4.2}$$

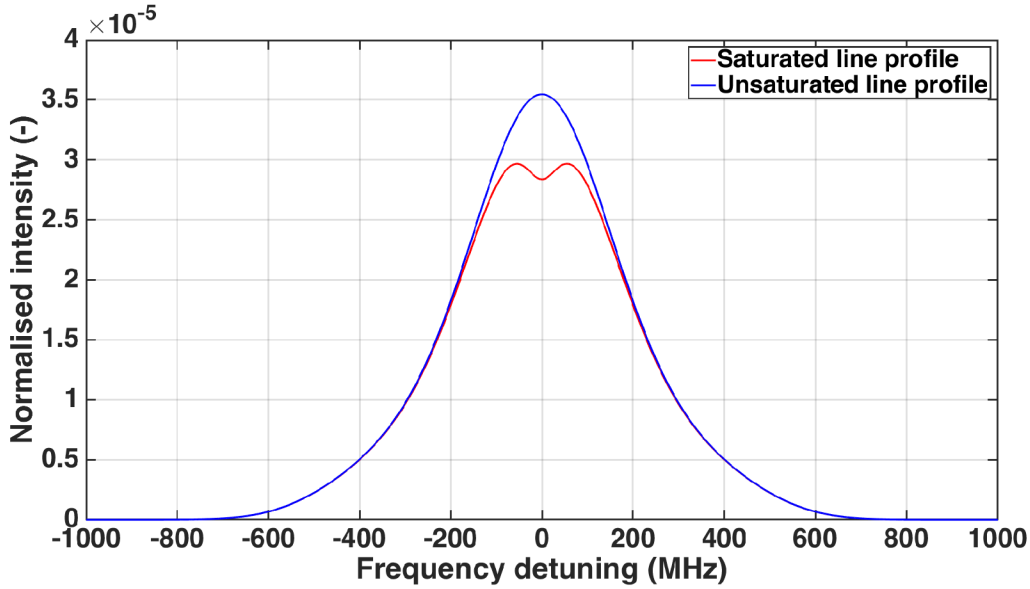

Figure 4.3: Comparison of the unsaturated and the saturated line profile.

where P stands for the pump beam power, A stands for the area of the pump beam, c stands for the speed of light in vacuum, B_{12} stands for Einstein coefficient of induced absorption, and R^* stands for an effective relaxation rate. The intensity for which the $S = 1$ is called the saturation intensity. It corresponds to the difference in population of higher and lower energy levels being half of the unsaturated value. The optimum of Lamb-dip S/N ratio is reached for $S \approx 1.4$. Further increase of the radiation intensity leads to the Lamb-dip broadening instead of improving the S/N ratio.

4.2.2. Limitation of the saturation absorption spectroscopy

While the saturation absorption spectroscopy overcomes the main limitation of the linear absorption spectroscopy precision, which is the Doppler broadening, another sources of the absorption line broadening can still be presente. Examples of such broadening can include: the time-of-flight broadening [23], the Stark broadening (caused by an external electric field), the Zeeman broadening (caused by a magnetic field), the collisional broadening, and many others.

The experimental setup overcoming these limits is becoming increasingly complex as the most accurate method for the absorption lines central frequency determination is to use the atomic (ion) clock [24], [25]. The ultimate restriction is the natural broadening caused by the finite time of life of electrons on energy levels.

5. State of art of $H^{13}C^{14}N$ precision spectroscopy

5.1. Linear absorption spectroscopy

5.1.1. Experimental arrangement of Sasada et al.

The first thorough study of $H^{13}C^{14}N$ $2\nu_3$ band to be mentioned was published by Sasada et al. [26] from Keio University in Japan in 1990. Authors studied HCN in the natural abundance and also enriched $H^{13}C^{14}N$ sample. Samples were prepared by reaction of H_2SO_4 and NaCN.

The laser used in the Sasada's article was a distributed feedback semiconductor laser (Hitachi HL1541A). Its radiation was split into several parts Fig. 5.1. The first part went through the 1 m long, 8 Torr CO reference cell. The second part went through 1 m, 1.3 Torr HCN absorption cell and the last part was sent to the Fabry-Perot (FP) interferometer (Tec-Optics SA-300). Photodiodes followed by lock-in amplifiers detected the beams transmitted through the absorption cells.

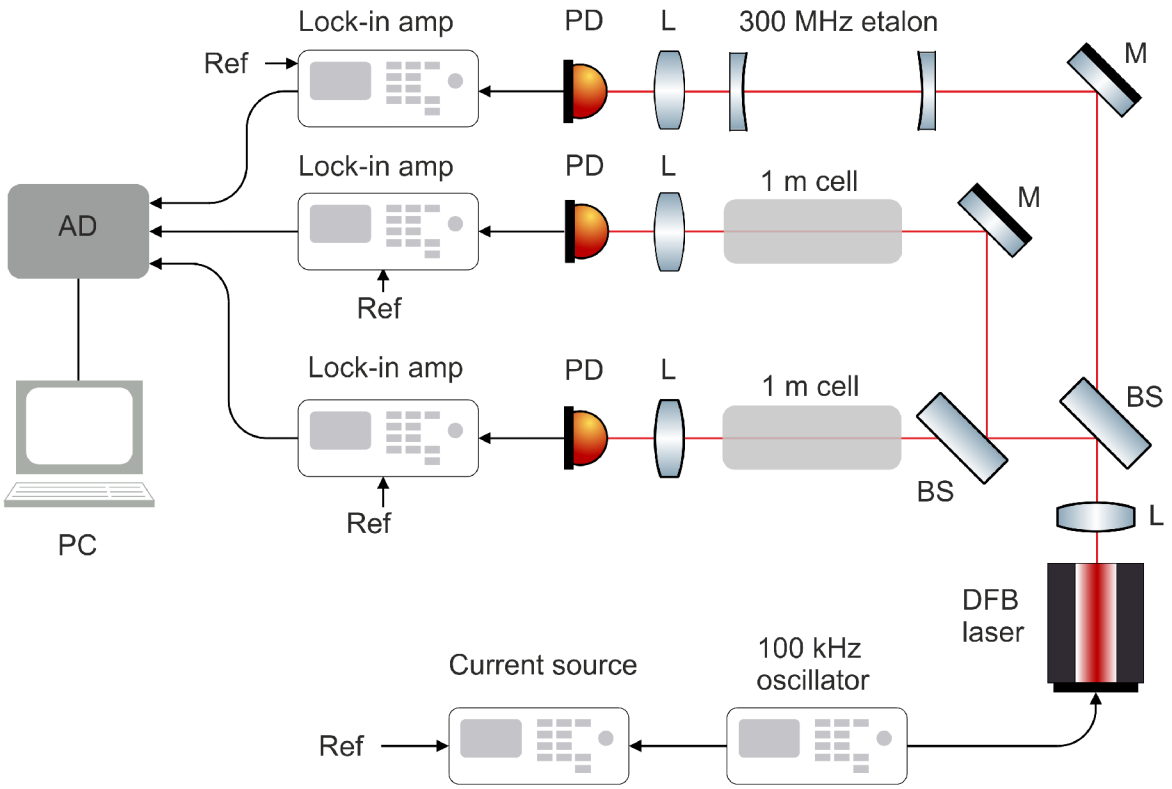

Figure 5.1: Experimental setup used in [26] for spectroscopy in HCN: amplifiers (AMP), analogue-digital (AD) converter, beam splitters (BS), computer (PC), distributed feedback (DFB) laser, lenses (L), mirrors (M), references (Ref).

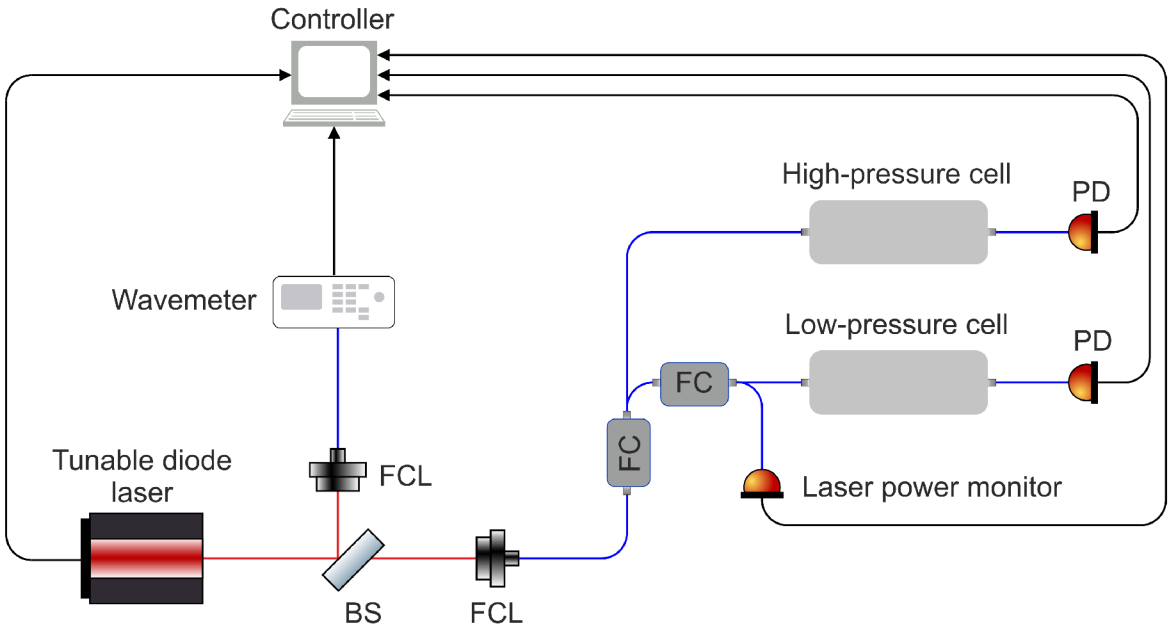

Figure 5.2: The experimental apparatus for the linear absorption spectroscopy measurement: beam splitter (BS), fibre collimators (FCL), fibre couplers (FC), photodetectors (PD). Adapted from [9].

Authors measured the band from 6380 to 6410 cm^{-1} ($\approx$ from 1567 to 1560 nm) with the absolute accuracy of 0.0005 cm^{-1} ($\approx$ 15 MHz) and the band from 6410 to 6570 cm^{-1} ($\approx$ from 1560 to 1522 nm) with the absolute accuracy of 0.0033 cm^{-1}. The lower accuracy was caused by using a less precise Michelson interferometer type of wavelength meter (Advantest TQ8325). The data were then combined with the data from [27] and [28] to perform least-square analysis to calculate molecular constant. These constants then served for the calculation of the absorption lines position for $2\nu_3$ and $2\nu_3 + \nu_2$ bands of $H^{12}C^{14}N$ and $H^{13}C^{14}N$ with the accuracy of 0.0005 cm^{-1} ($\approx$ 15 MHz) for the intense lines and lower accuracy up to 0.0021 cm^{-1} ($\approx$ 63 MHz) for less intense lines. The pressure shift effect was estimated to be lesser than the presented accuracy of the wavenumber measurement.

5.1.2. Experimental arrangement of Swann et al.

The most up-to-date study of $H^{13}C^{14}N$ $2\nu_3$ band was done by Swann and Gilbert in [9]. They used a very similar setup Fig. 5.2 to the one they used in [29] with the addition of a FP filter (cavity), narrowing the scanning laser frequency line. The absorption cells were 0.13 kPa and either 3.3 kPa or 6.0 kPa. All of the cells were 15 cm long with windows attached to the cell by a glass frit method. The windows were mounted at an angle of 11° and wedged by $\approx 2°$ to prevent the interference fringes in the transmitted signal. The cells were filled with the $H^{13}C^{14}N$ produced by the reduction of 99 % isotopically pure potassium cyanide with a stearic acid under the vacuum and a mild heat ($\approx$ 80 °C).

The accuracy of the wavelength meter was tested by measuring rubidium hyperfine components. The frequency of the laser stabilised to the rubidium line was measured by comparison with the optical frequency comb [30]. The uncertainty combined as the

calibration uncertainty and uncertainty of wavelength meter drift between calibrations was 0.004 pm (≈ 0.5 MHz) @ 1560 nm).

The linearity of the wavelength meter was verified by measuring $^{12}C_2H_2$ lines between 1528 nm and 1538 nm. The lines were measured the same way as the HCN lines described in the [29], and the results were compared with those in [31], with the average results being in 0.002 pm agreement.

The pressure monitoring in the absorption cells was allowed by the previous measurement of the P16 absorption line pressure broadening dependence on the pressure. In the case of a low-pressure cell, authors reported an exponential decay in the pressure from 0.133 kPa to 0.106 kPa over the nine-day duration of the measurement. They mention as the likely reason the adsorption of HCN on the cell surface.

Twenty-five absorption lines were measured and extrapolated to zero pressure with the uncertainty varying from 0.000 01 nm (≈ 1.2 MHz) to 0.000 027 nm (≈ 3.4 MHz). Authors also determined the pressure shift coefficients and the pressure broadening coefficients of these twenty-five lines. The measured line centres corresponded well with the data measured in [26].

The position of twenty-five measured lines was used for the calculation of the molecular constants for ground and excited states and served for the calculation of the position of fifty-six $H^{13}C^{14}N$ absorption lines. The uncertainty was from 0.000 008 nm (≈ 1.0 MHz) to 0.000 025 nm (≈ 3.1 MHz).

5.1.3. Practical use of the linear absorption data

Authors in [7] used $H^{13}C^{14}N$ absorption cells as the length reference in their frequency scanning interferometer. During the gas cell calibration procedure, they found out the correlated term in the uncertainty of the $H^{13}C^{14}N$ absorption lines' centre at different pressures. It indicates that certain shifts might be present in the data published in [9].

In the article [32], authors used $H^{13}C^{14}N$ and $^{12}C^{16}O$ absorption cells as an inexpensive traceable method for the calibration of the ladar system. They stated that the "conservative" systematic uncertainties of the absorption lines positions represented limitations for their calibration's accuracy.

The $H^{13}C^{14}N$ was also used in [33] and [34] as wavelength reference for the fibre Brag grating demodulation. It shows that the linear absorption spectroscopy of $H^{13}C^{14}N$ represents a useful tool for many applications, even though more accurate data would help further improve its benefits for the scientific as well as the industrial community.

5.2. Saturation absorption spectroscopy

5.2.1. Experimental arrangement of Labachelerie et al.

The first experiment (up to my best knowledge) regarding the saturation absorption spectroscopy in $H^{13}C^{14}N$ was described in [35]. Authors used an external cavity semiconductor laser (Littrow configuration) Fig. 5.3, allowing the initial 120 nm tuning range. The tuning range was limited by the glueing of mechanical supports restricting the range to 1.51-1.58 μm. The absorption cell was a 20 cm long FP cavity with 99 % reflectivity of the input and the output mirror. The laser current was frequency modulated at 1 kHz

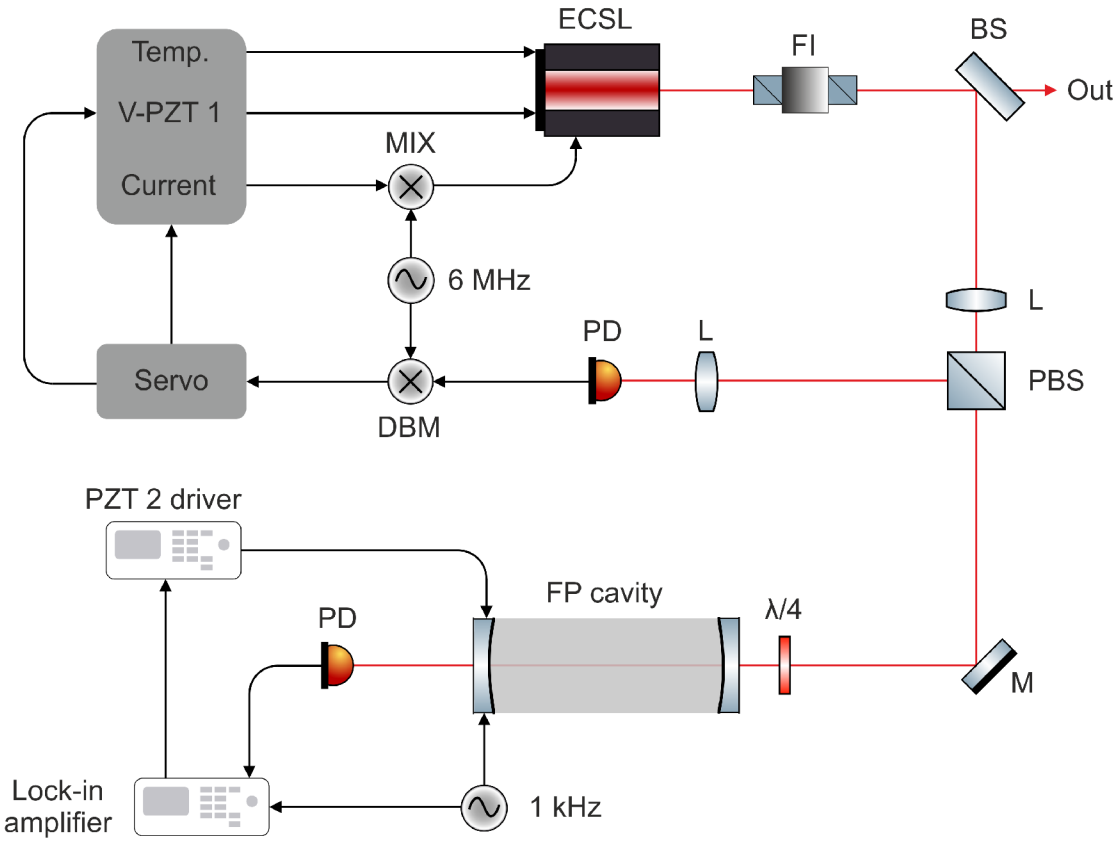

Figure 5.3: Experimental setup for saturation absorption spectroscopy in acetylene and hydrogen cyanide: beam splitter (BS), double-balanced mixer (DBM), external cavity semiconductor laser (ECSL), Fabry-Perot (FP) cavity, Faraday isolator (FI), piezo crystals (PZT), polarising beam splitter (PBS), quarter-wave plate ($\lambda/4$). Adapted from [35].

with the modulation depth of 6 MHz. While the laser frequency was locked to FP cavity resonance, it could be tuned by ≈ 1 GHz using the piezo-crystal.

The experiments were conducted with $^{12}C_2H_2$, $^{13}C_2H_2$ and HCN (what hydrogen cyanide isotope was used authors do not mention). The cavity was filled with the 10-20 mTorr of acetylene (the pressure used in HCN experiments is not noted), and "many" sub-Doppler lines were recorded. The successful saturation of P27 $^{13}C_2H_2$ and P27 HCN absorption lines serves as an example. Authors also calculated the relative stability of the laser locked to a minimum of P13 $^{12}C_2H_2$ with the best stability of 10^{-12} reached at an integration time of ≈ 1 s.

Further research led to the publication [36]. In this work authors upgraded the experimental setup Fig. 5.3 and measured the $H^{12}C^{14}N$ P27 line with the uncertainty of 0.1 MHz.

5.2.2. Experimental arrangement of Henningsen et al.

Authors from the Danish Fundamental Metrology (DFM) were dealing with the saturation spectroscopy of the acetylene and the hydrogen cyanide in photonic bandgap fibres [37]. They used an external cavity laser amplified by an erbium-doped fibre amplifier (EDFA) to 60 mW. The radiation went through the hollow-core photonic bandgap fibre (HC-PBG) with the 7-cell core of 10 μm diameter located in a vacuum box.

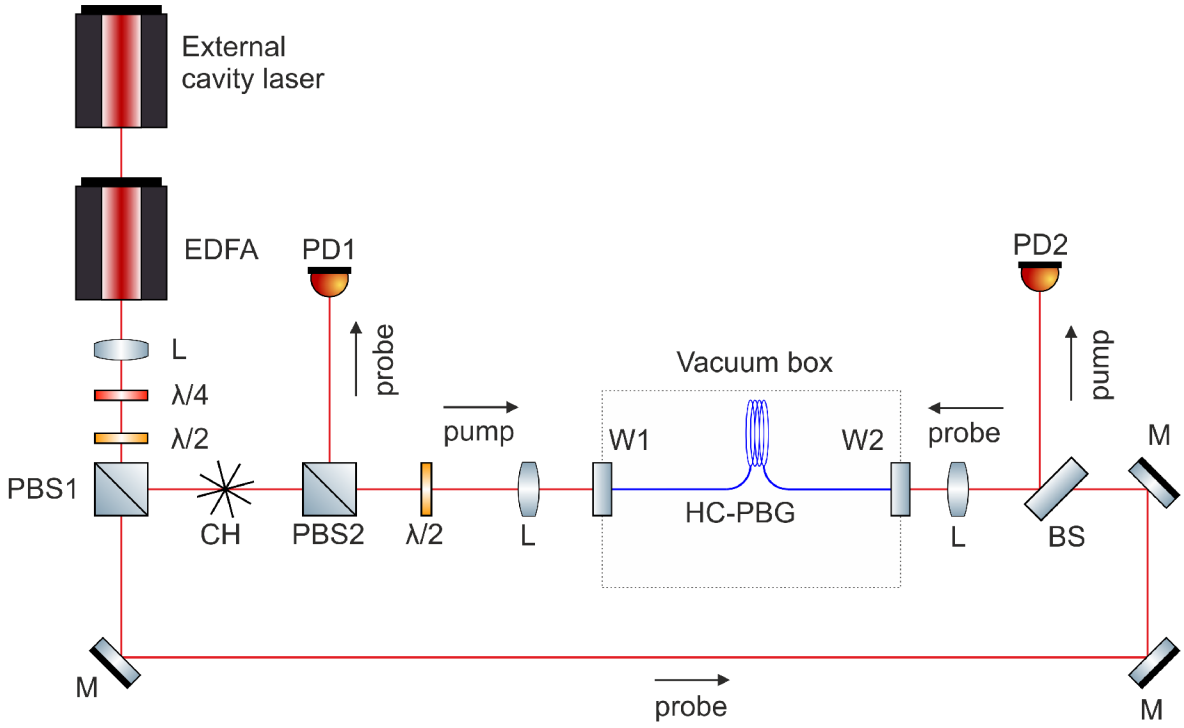

Figure 5.4: Experimental setup for the saturation absorption spectroscopy in the hollow-core fibre: beam splitter (BS), chopper (CH), erbium-doped fibre amplifier (EDFA), half-wave plates ($\lambda/2$), hollow-core photonic bandgap fibre (HC-PBG), lenses (L), mirrors (M), photodetectors (PD), polarising beam splitters (PBS), quarter-wave plate ($\lambda/4$), sapphire windows (W)). Adapted from [37].

Three different detection schemes were used. In the first case, the transmitted signal through the hollow-core fibre was detected close to the window W2 by 5x5 mm^2 Ge detector. The second configuration included an aspherical lens with 13 mm focal length focusing the exit beam and a mirror placed in the focal plane reflecting the beam back into the fibre. The mechanical chopper (CH) was placed in front of the mirror. The Ge detector monitored the signal chopped at 670 Hz frequency. The signal from the detector was subsequently demodulated in a lock-in amplifier.

The third version of the experimental setup is shown in Fig. 5.4. The laser beam transmitted by PBS1 (polarising beam splitter) served as a counter-propagating beam through the hollow-core fibre. The described laser beam is called probe beam and it was measured at the PD1 (photodetector). The PD2 monitored the pump beam.

The experiments with the 6.35 m long HC-PBG filled with $H^{13}C^{14}N$ showed different results to those of acetylene. In the case of hydrogen cyanide, after filling the fibre, the pressure started to drop exponentially. Authors attributed the exponential drop to the permanent dipole moment of the $H^{13}C^{14}N$ molecule, that causes the tendency of the gas to "stick" to the fibre wall.

Authors successfully measured the saturation absorption signal for the P9 C_2H_2 (however, they do not mention the used isotope) and R7 $H^{13}C^{14}N$. The dominating broadening mechanism in their measurement was transit-time broadening, causing the measured lines to have HWHM of ≈ 20 MHz.

Presented article illustrates authors' effort to use the saturation absorption spectroscopy for $H^{13}C^{14}N$ absorption lines measurement. The restricting factor seems to be the permanent dipole moment of the molecule. It causes the decrease of an "effective" pressure in the absorption cell (the hollow-core fibre) given that molecules "stick" to the fibre walls [38]. Therefore, this might be the reason why no systematic measurement of $H^{13}C^{14}N$ absorption lines centre using the saturation absorption spectroscopy has not been performed so far.

6. Linear absorption spectroscopy

6.1. First harmonic detection method

6.1.1. Preliminary experiment with the Koheras Adjustik laser

At the first stage of my research on the measurement of $H^{13}C^{14}N$ absorption lines, I used a simple linear absorption setup with the Koheras Adjustik E15 laser. The laser beam went three times through the gas cell (67 Pa nominal pressure, 20 cm length, Wavelength References, Inc.) and hit the photodetector (PD). The reference signal was monitored on the other PD. This allows the use of the technique, that eliminates the residual amplitude modulation (RAM) [39]. The laser frequency was modulated and subsequently demodulated on first harmonic frequency.

The optical frequency comb (OFC) [40] was filtered through the Brag grating, reflecting only a specific part of the OFC spectrum. The OFC is then combined with the laser beam. The combined beam then hit the PD, and after being frequency filtered, the beat-note frequency was measured by the counter. The laser was locked to the absorption line minimum, and the frequency of the absorption line minimum was calculated from the beat-note record.

Used Adjustik laser's tuning range is approx. from 1539.8 nm to 1541.0 nm. That permitted me to measure a single absorption line of $H^{13}C^{14}N$, concretely R2. The difference between my measurement [41] and the results published in [9] was about 0.9 MHz, while the relative stability of a laser locked to the minimum of R2 line was 10^{-8} at 8 hours integration time.

6.1.2. Experiments with the CTL 1550

Further improvements in the experimental configuration in 6.1.1 led to the setup Fig. 6.1. The Koheras Adjustik E15 laser was replaced by a newly acquired continuously-tunable laser (CTL 1550, TOPTICA Photonics AG) with built-in Faraday isolator. The CTL 1550 allows for a mode-hop free frequency tuning in the range from 1510 nm to 1630 nm. This range is covering the whole absorption spectrum of $H^{13}C^{14}N$. The optical power of the CTL was stabilised by a variable optical attenuator (VOA). The VOA is getting an error signal from the proportional–integral–derivative (PID) controller. In order to create an error signal, the signal from the reference output of the double-balanced photodetector (DBPD) (Nirvana 2017, Newport) is used. The combination of the Glan-Taylor crystal (GT) and a half-wave plate ($\lambda/2$) ensured the polarisation stability of the laser beam entering the experimental setup.

I used the absorption cell (0.4 Torr nominal pressure, 40 cm length, Wavelength References, Inc.), with the wedged windows. The windows had an anti-reflective (AR) coating and were fitted to the tube at a slight tilt to minimise the interference effects. The cell was covered in a custom-made temperature-controlling device, minimising the pressure changes in the cell caused by temperature changes. The PID controller regulated the temperature through four Peltier heaters attached to an aluminium cover. The cover was in thermal contact with the glass cell. The temperature-controlling sensor was located inside the aluminium cover. The sensor measured the temperature stability in the order of 10 mK, ensuring that the temperature-induced pressure effect on the gas was negligible.

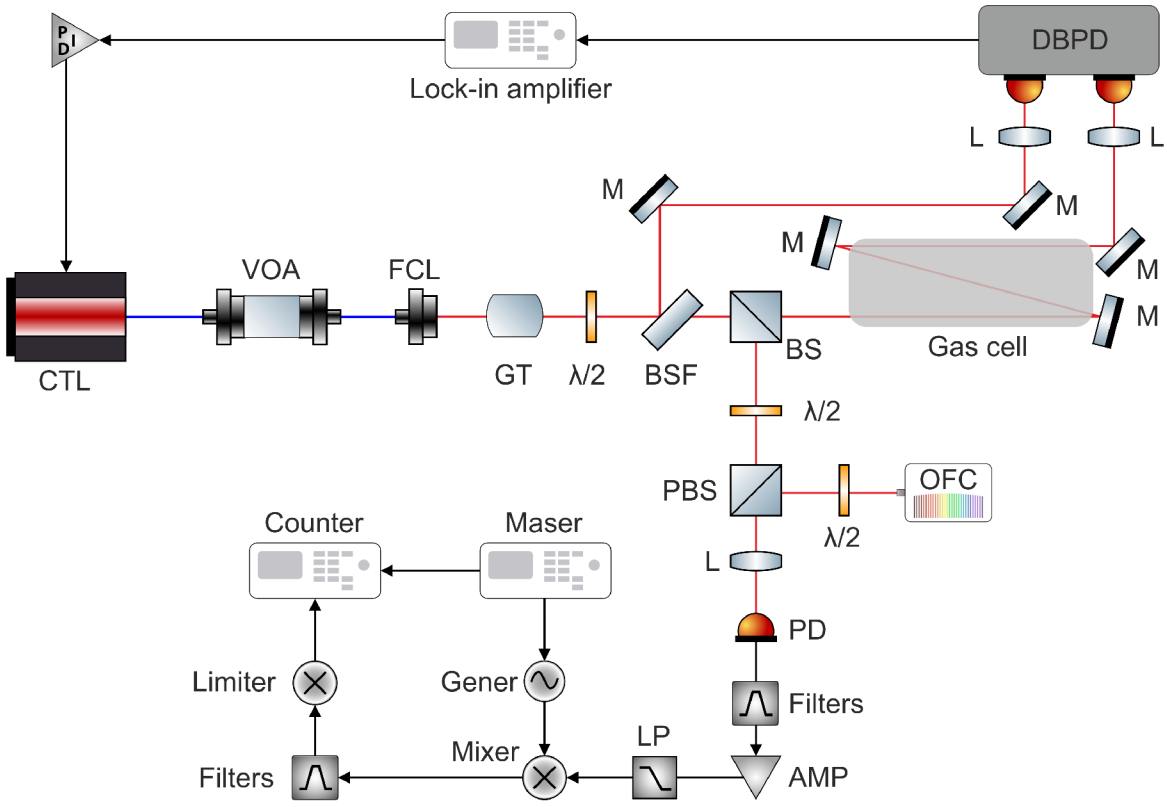

Figure 6.1: The experimental setup for the linear spectroscopy measurement: band pass filter (BP), beam sampler (BSF), beam splitter (BS), continuously-tunable laser (CTL), double-balanced photodetector (DBPD), fibre collimator (FCL), Glan-Taylor crystal (GT), half-wave plates ($\lambda/2$), lens (L), low pass filter (LP), mirrors (M), photodetector (PD), polarising beam splitter (PBS), and variable optical attenuator (VOA). Adapted from [44].

In this measurement, I used the double-balanced photodetector to minimise the noise introduced to an optical signal. The laser frequency was modulated at 10 kHz with the 6 MHz modulation depth. The lock-in amplifier referenced by active hydrogen maser [42] demodulated the signal at the first harmonic frequency.

A part of the laser beam was combined with an optical frequency comb [40], and the resulting beat-note frequency was filtered and measured by counter. The counter was referenced to an active hydrogen maser [42]. The whole experimental setup was covered in a thermal insulation box (MIRELON), minimising the temperature changes in the optical part of the setup.

The CTL frequency was locked to the minimum of a certain absorption line and kept in lock typically for about 8 hours. A representative example Fig. 6.2 of the Allan deviation [43] shows the stability of about $9{*}10^{-12}$ at 1 min integration time. It represents three orders of improvement compared to the results presented in [41].

Thanks to the experimental configuration described above, I was able to measure twenty-six absorption lines with the 2σ standard deviation between 40 kHz and 70 kHz [44]. While I reached the limit of the linear absorption method regarding the laser frequency stability, the crucial task to improve was the repeatability of the results. The repeated measurement of the same line within a long-term interval ($\approx$ week) between

each measurement showed the absolute frequency of a line centre fluctuation in 1 MHz order.

Further linear absorption spectroscopy research led to the modulation-free absorption technique, which will be described in the next section.

6.2. Modulation-free spectroscopy

Only the tiny surrounding of the absorption lines minimum is monitored while using the modulation techniques for the determination of the absorption lines centre (the modulation depth in [44] was 6 MHz). As further enlargement of modulation depth brings more disadvantages (e.g. the modulation broadening of the absorption lines, the residual amplitude modulation), the idea of using a modulation-free spectroscopy came to light. The monitored part of the line can be easily changed, this makes a clear advantage over techniques using a frequency modulation. To determine the absorption line centre, wider part of the absorption line was involved.

The modified setup for modulation-free absorption lines measurement can be seen in Fig. 6.3. The frequency of the CTL was locked to the particular tooth of OFC using a phase locked loop (PLL), as described in [45]. The OFC absolute frequency was maintained by continuously tracking a global navigation satellite system (GNSS). Thanks to that, the frequency of the CTL was known with fractional uncertainty at 10^{-13} order and controllable down to 10^{-15} order. Given that it is possible to control the offset between the CTL and the OFC tooth frequency, the CTL frequency can be constantly scanned over the absorption line profile.

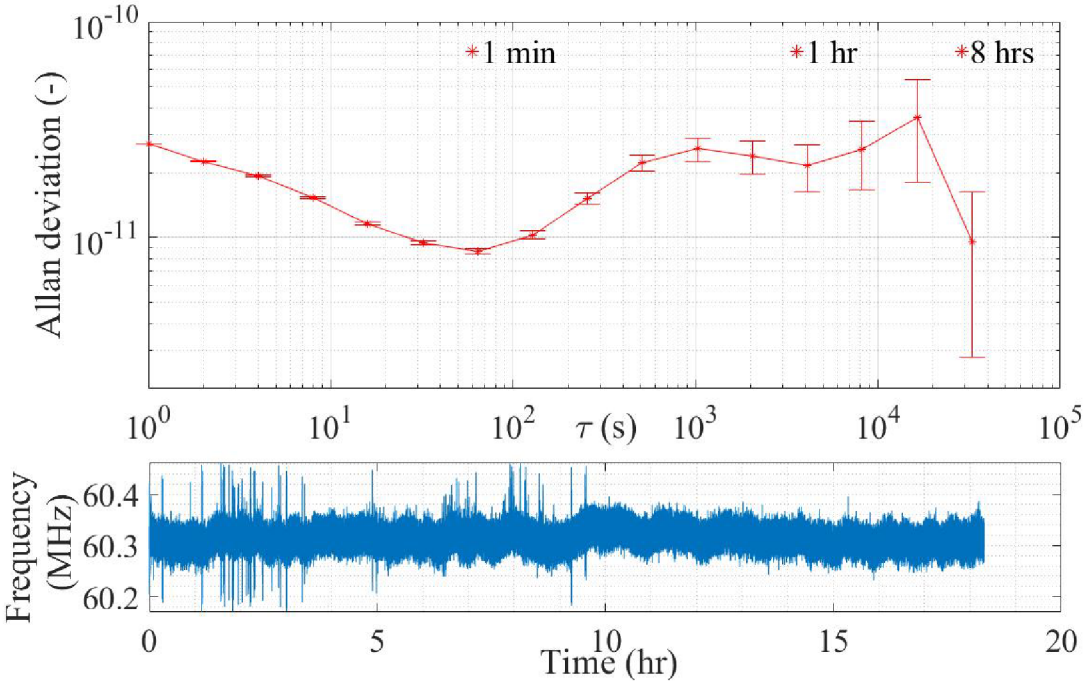

Figure 6.2: The Allan deviation (upper figure) calculated from the time evolution of laser frequency locked to the minimum of $H^{13}C^{14}N$ R6 absorption line. Adapted from [44].

Table 6.1: The pressure shift coefficients determined by the linear absorption spectroscopy compared to the results published in [9].

Line	k_{ISI} (MHz/Torr)	dk_{ISI} (MHz/Torr)	k_{SW} [9] (MHz/Torr)	dk_{SW} [9] (MHz/Torr)
R23	- 1.31	1.34	- 1.02	0.03
R18	- 1.44	0.26	- 1.45	0.03
R12	- 1.05	0.16	- 0.98	0.03
R10	- 0.45	0.10	- 0.45	0.03
R9	- 0.06	0.12	- 0.09	0.02
R8	0.08	0.10	0.35	0.09
R7	0.48	0.16	0.58	0.12
R5	1.28	0.21	1.39	0.03
R3	1.64	0.28	1.87	0.04
P4	- 1.44	0.26	- 1.52	0.03
P5	- 1.30	0.20	- 1.40	0.03
P10	0.27	0.09	0.40	0.02
P16	1.93	0.29	2.30	0.06
P20	2.09	0.57	2.49	0.09
P24	1.48	1.23	2.06	0.03

A feedback loop maintained the power stability of the laser, and the PD detected and monitored the power fluctuation. The acousto-optic modulator (AOM) served as the active element. The setup included two absorption cells (0.4 Torr nominal pressure, 40 cm length, Wavelength References, Inc. and 2 Torr nominal pressure, 40 cm length, Wavelength References, Inc). The use of two absorption cells simultaneously allowed me to calculate the pressure shift coefficient for each measured absorption line.

The profiles of fifteen absorption lines were scanned with the step of 1 MHz (50 kHz around the central part of the profile). The measured absorption line profile was then fitted, and the position of the absorption lines minimum was recovered with an uncertainty in the order of 100 kHz. Despite all of the attempts to improve the repeatability of the measurement, the problems with the (time-dependent) background in the measured spectrum remained. It shifted the absorption lines' positions by order of 100 kHz. The pressure shift coefficients, that were measured using two absorption lines Tab.6.1 corresponded to the coefficients presented in [9] Fig. **??**.

Compared to [9], higher uncertainty is caused by the use of only two absorption cells to determine the pressure shift coefficients. Authors employed about ten cells and the least-square method to obtain coefficients. Furthermore, the relative pressure uncertainty in our cells was 10 %, limiting the measurement precision.

The problem with the background in the absorption spectrum remained, causing troubles by shifting the measured position of $H^{13}C^{14}N$ absorption lines centre. The theoretical calculations, in which I compared the fitting of the Gauss profile with and without modelled background, showed that the background should not be more than 0.01 % of signal for highly absorptive lines and 0.001 % for low absorptive lines. My conclusion corresponds with the [46], where the authors say: "Expending only reasonable effort, the line centre of a pressure broadened line typical of a molecular absorption wavelength reference cannot be defined to better than about ± 0.01 pm". It corresponds to $\approx$1 MHz at $\lambda = 1550$ nm.

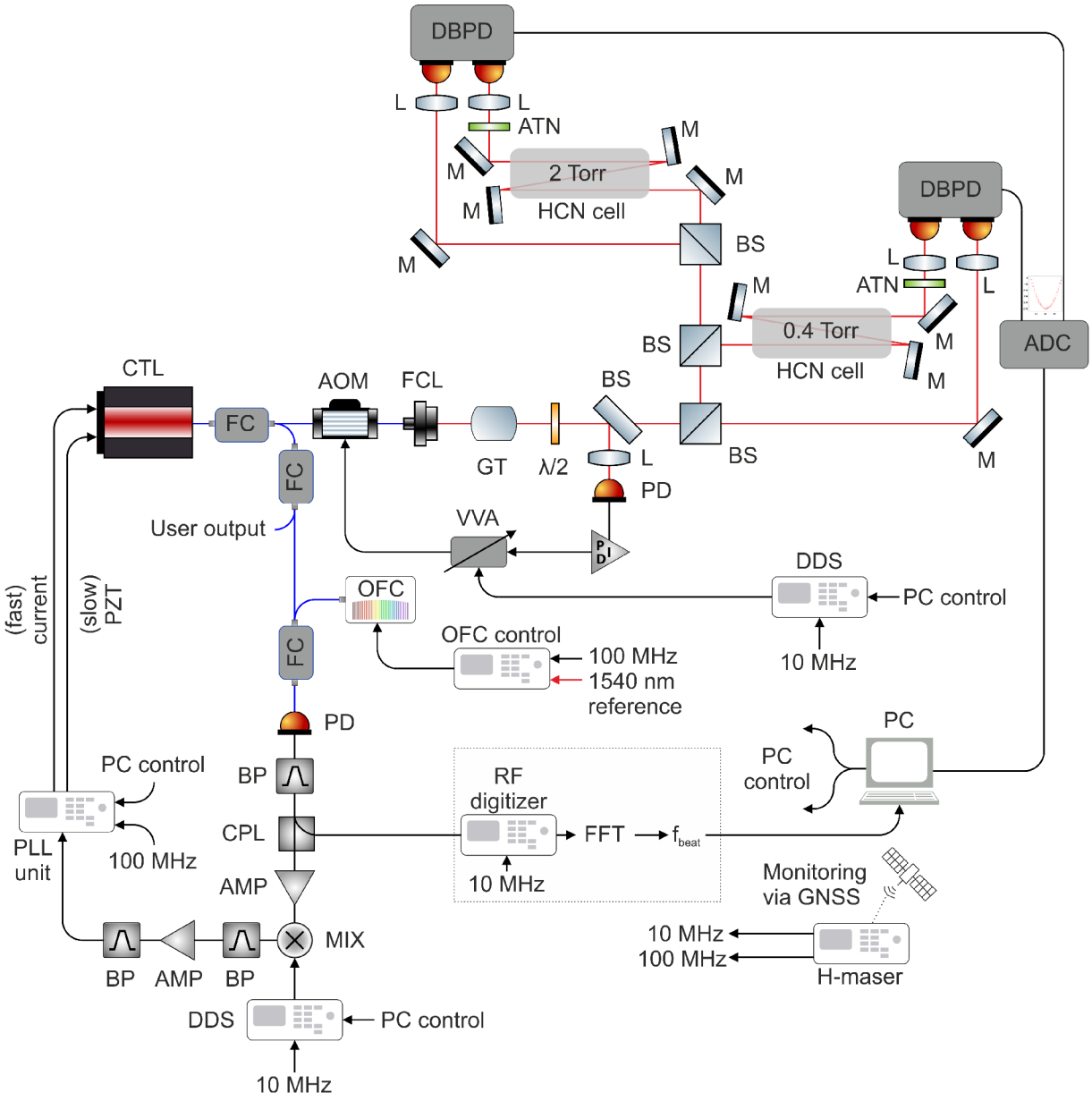

Figure 6.3: An experimental setup for modulation-free $H^{13}C^{14}N$ absorption lines centre measurement: acousto-optic modulator (AOM), amplifiers (AMP), analogue-digital converter (A/D), attenuators (ATN), band pass filters (BP), beam splitters (BS), continuously-tunable laser (CTL), direct digital synthesiser (DDS), double-balanced photodetector (DBPD), fast Fourier transform (FFT), Glan-Taylor crystal (GT), half-wave plates ($\lambda/2$), lenses (L), mirrors (M), optical frequency comb (OFC), phase locked loop (PLL) unit, photodetector (PD), polarising beam splitter (PBS), proportional–integral–derivative (PID) controller, radio frequency (RF) digitiser card, radio frequency coupler (CPL), radio frequency mixer (MIX), and voltage variable attenuator (VVA). Adapted from [45].

Further research was focused on the saturation absorption spectroscopy, permitting a high background suppression [47], as well as Doppler-free profile measurement.

7. Saturation absorption spectroscopy

Before the first attempts for the saturation absorption spectroscopy measurements in $H^{13}C^{14}N$, I calculated a saturation coefficient S (described in the section 4.2.1). The needed relaxation coefficient was taken from [48] and HCN partition function from [49]. The results showed two options, either to use high optical power to saturate the energy transitions in $H^{13}C^{14}N$ or to use low pressure of $H^{13}C^{14}N$. As the low-pressure absorption cells of HCN are not commercially available, the first attempts were performed with a high optical power.

7.1. High optical power approach

The instrumental equipment at the Institute of Scientific Instruments (ISI) includes a Koheras Boostik amplifier, that produces enough optical power for my experiment. The amplifier was seeded by the Koheras Adjustik E15 diode laser, which permitted to measure a single absorption line of $H^{13}C^{14}N$ (R2 line) at 1540.431 20 nm. The sketch of the experimental setup can be seen in Fig. 7.1.

To optimise the optical power propagating into the experimental setup, the half-wave plate ($\lambda/2$) and the polarising beam splitter (PBS) were combined to easily lower and to absorb the excessive optical power by a beam-dump (BD). The laser beam then went through the telescope. The telescope lowered the diameter of the beam to 2.5 mm. The beam with a lowered diameter could then pass through the Faraday isolator (FI). The FI afterwards protected the laser from the back-scattered light. The R2 absorption line of $H^{13}C^{14}N$ was saturated by 492 mW pump beam and then measured by 61 mW probe beam. After crossing the gas cell, the pump beam was absorbed by the BD. The probe beam hit the double-balanced photodetector (DBPD) (Nirvana 2017, Newport), subtracting the noise in the signal branch using the reference branch signal. The 0.5 m long gas cell was filled with 0.4 Torr (about 53 Pa) $H^{13}C^{14}N$. The laser frequency was modulated at 1.26 kHz modulation frequency with modulation depth $\approx$ 7.5 MHz. The detection was done by a lock-in amplifier at the third harmonic frequency.

The signal was monitored on the oscilloscope. Due to high pump power, the absorption line was power-broadened ($\approx$ 20 MHz full width at half maximum), and the modulation depth needed for optimal signal-to-noise (S/N) ratio was too high. Due to this facts the recorded signal was only ilustrative and can not be under any circumstances used for determining the position of the absorption line centre. The third harmonic signal at the crossing with the scanning signal showed an s-shape curve, that corresponds to the saturated line profile. This result confirmed that it is possible to measure the saturated absorption in $H^{13}C^{14}N$. However, it was necessary to decrease the gas pressure so that the pump beam optical power could be lowered too.

7.2. Low gas pressure approach

7.2.1. Preliminary experiments

The absorption cell used in the high optical power approach (0.4 Torr pressure) is a cell with the lowest pressure available on the market (up to my knowledge). The lowest pressure cell possesses a still too high pressure to be applied for the saturation absorption spectroscopy in order to determine the absorption lines' centre. After a detailed analysis of the possible solutions, a high-pressure vessel connected to a vacuum setup seemed to fix the issue.

The gas reservoir was connected to the rest of the setup through a needle valve, allowing fine dosing of the absorption cell. I was able to monitor the gas pressure filled in the cell with the uncertainty of about 3 % thanks to the combination of the low precision wide-range vacuum gauge and the precise low-range capacitance vacuum gauge. Before filling the cell, it was evacuated by the turbomolecular vacuum pump. The cell was connected to the rest of the setup through a below, that protected the cell from being stretched or strained.

When the vacuum part of the experimental setup was built, I focused on building the optical part Fig. 7.2. The experimental configuration was similar to that presented

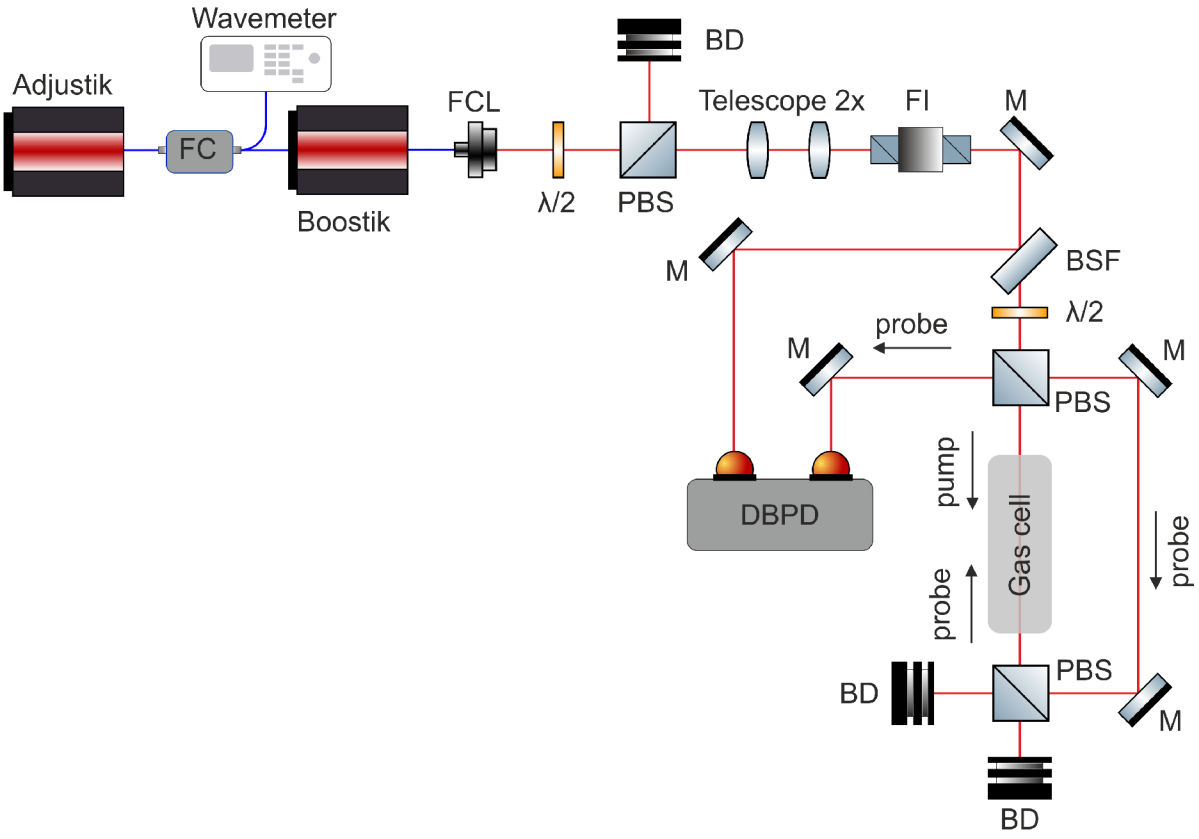

Figure 7.1: A saturation absorption spectroscopy setup based on the Koheras Boostik amplifier: beam-dumbs (BD), beam sampler (BSF), double-balanced photodetector (DBPD), Faraday isolator (FI), fibre collimator (FCL), fibre coupler (FC), half-wave plates ($\lambda/2$), mirrors (M), polarising beam splitters (PBS).

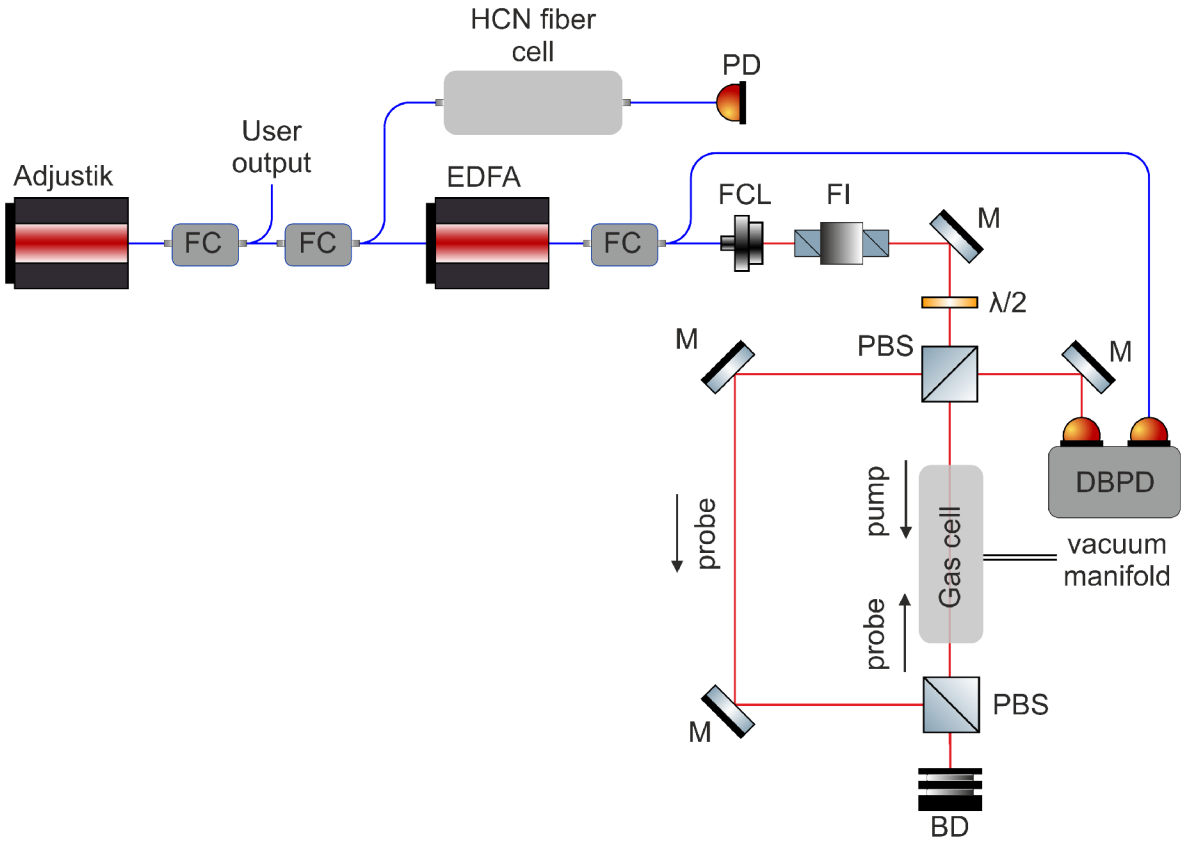

Figure 7.2: The optical part of the experimental setup for the saturation absorption spectroscopy in $H^{13}C^{14}N$: beam-dump (BD), double-balanced photodetector (DBPD), erbium-doped fibre amplifier (EDFA), Faraday isolator (FI), fibre collimator (FCL), fibre couplers (FC), half-wave plate ($\lambda/2$), mirrors (M), polarising beam splitters (PBS), photodetector (PD). Adapted from [50].

in Fig. 7.1. The main difference was that the erbium-doped fibre amplifier (EDFA) replaced the Boostik as the needed optical power was lower (≈100 mW). The fibre cell was filled to 25 Torr (Wavelength References, Inc.) and served as reference to ensure that the wavelength of the laser corresponded to the wavelength of the absorption line centre.

The absorption cell during the first experiments (described in [50]) was filled to pressure 1-5 Pa, and the laser was modulated through the piezo with 1 kHz modulation frequency and 6 MHz modulation width. The pump power was about 130 mW and the probe beam power about 3.5 mW. I used the synchronous demodulation technique to obtain the third harmonic signal of the absorption line.

As I managed to record the first third harmonic signal, the problems with the S/N ratio degrading in time occurred. Up to my best knowledge, the reason behind this is the permanent dipole moment of HCN molecules, which makes them adsorb to the absorption cell walls. The effect is briefly mentioned in [37] but was not systematically studied. At first, the adsorption effect was pretty fast, as the S/N ratio of the third harmonic signal dropped to 50 % in about 45 minutes Fig. **??**. It made the signal hardly usable for the absorption line centre determination, as the "effective" pressure in the cell was rapidly changing through the measurement.

7.2.2. Molecule adsorption suppression

Saturating the gas cell wall by filling the cell with $\approx 10\,\mathrm{Pa}$ constituted the first attempt to remove the adsorption effect. After being filled up, the cell remained still for several days, and then the pressure was reduced to $\approx 2.5\,\mathrm{Pa}$. The error signal was then monitored, but unfortunately, no "presaturation" effect was observed.

The following attempt was to activate the inner walls of the cell by perfusion with an ozonised air for 90 minutes, with $\approx 50\,\mathrm{mg/h}$ of ozone. Then, the cell was filled with 1 % solution of chlorotrimethylsilane (Aldrich, >98 % by GC) in methanol (Penta chemicals, p.a.). Thereafter, the cell was incubated for 90 minutes at a room temperature. The solution was then discarded. The cell was thoroughly washed with pure methanol, blow-dried with a filtered air, and simultaneously heated to about 50 °C with a hot air gun (as described in [8]). It led to decline of the adsorption effect, so the S/N ratio of the third harmonic signal dropped to 50 % in about 6.5 hours Fig. 7.3. Anyway, further investigation on minimising the adsorption effect would be beneficial. However, given the lenght of my doctoral studies, I was not able to dedicate to this.

7.2.3. Table of $H^{13}C^{14}N$ absorption lines

Finally, further optimisation of the experimental conditions led to publication [8]. I utilised a continuously-tunable laser (CTL 1550, TOPTICA Photonics AG) with the build-in Faraday isolator as the laser source Fig. 7.4, which allows for mode-hop free tuning across the range from 1510 nm to 1630 nm. The CTL's optical frequency was locked to the particular tooth of the optical frequency comb (OFC) with the desired frequency offset. As the frequency offset was tunable, it permitted to tune the CTL frequency and to scan the absorption line profile (the offset lock was described in detail in [45]). The CTL's frequency was known with a relative accuracy of 10^{-13} and could be controlled down to the 10^{-15} level. The repetition frequency of the OFC (250 MHz)

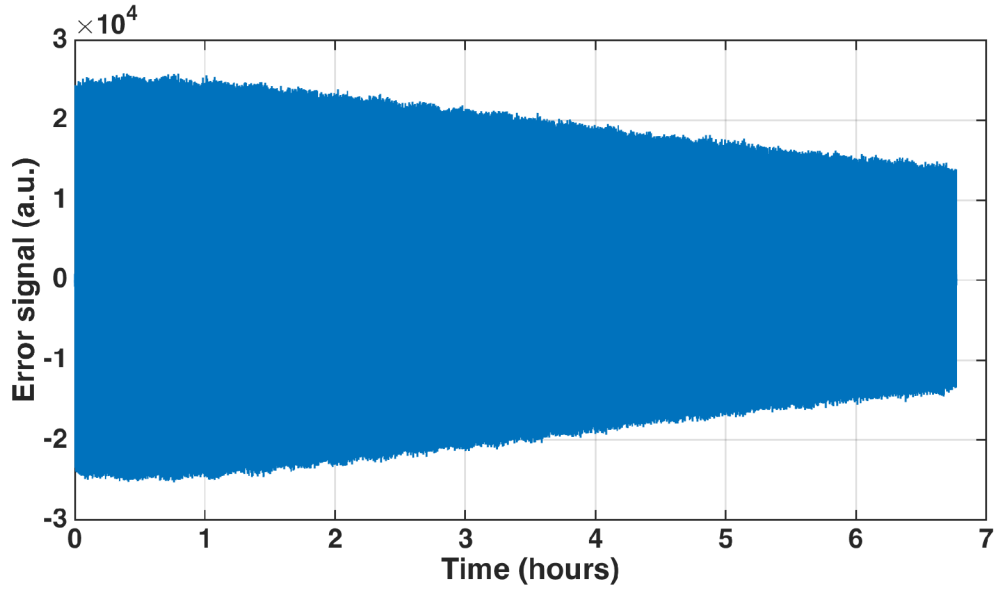

Figure 7.3: The decay of the third harmonic detection signal in time after passivisation of inner walls of the gas cell. Adapted from [50].

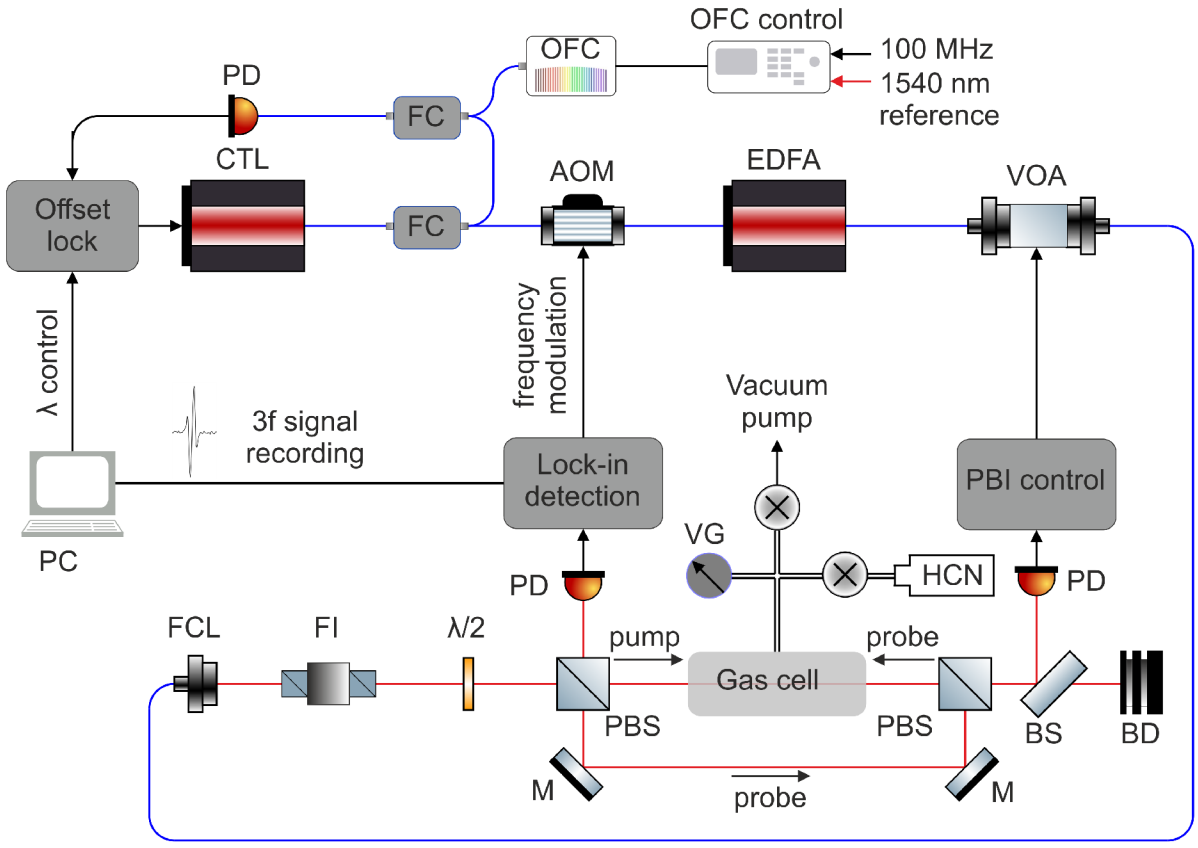

Figure 7.4: The experimental arrangement for the saturation absorption spectroscopy: acousto-optical modulator (AOM), beam-dump (BD), beam sampler (BS), computer (PC), continuously-tuneable laser (CTL), erbium-doped fibre amplifier (EDFA), Faraday isolator (FI), fibre collimator (FCL), fibre coupler (FC), mirrors (M), optical frequency comb (OFC), photodetectors (PD), polarising beam splitters (PBS), probe beam intensity (PBI), vacuum gauge (VG), variable optical attenuator (VOA). Adapted from [8].

was referenced by H-maser (described in [42]). The absolute frequency of the H-maser was continuously tracked to a global navigation satellite system (GNSS) time. The GNSS tracing was enabled by the time transfer receiver instrument. Furthermore, the absolute frequency of the H-maser was non-periodically compared to the frequency of a $^{40}Ca^{+}$ ion optical clock [51].

The optical power coming from the CTL was frequency-modulated using AOM. The modulation frequency was 5 kHz, the modulation depth 3 MHz. The laser beam was then amplified by EDFA and power stabilised using the variable optical attenuator (VOA, V1550PA, Thorlabs). The pump beam power was kept at ≈120 mW and the probe beam power at ≈10 mW with a beam diameter of about 2.3 mm. The absorption cell was 40 cm long stainless steel tube with fused silica optical windows glued to the cell body by vacuum-compatible glue. Its inner surface was treated as described in the section **??**. The pressure in the cell was kept between 1.45 Pa and 1.8 Pa, and the cell was refilled once every ≈ 0.5 hour.

The probe signal was synchronously demodulated using a digital lock-in amplifier (SRS 865, Standford Research Systems) and the third harmonic signal was detected. Each

absorption line scan was performed in the range of ± 12.5 MHz around the absorption line centre with the step of 1 kHz around the centre and 5 kHz at the rest of the scan. The points around the central part of the profile were then interpolated by linear function to detect the zero-crossing, which corresponds to the absorption line centre. This way, I was able to measure fifty-six absorption lines of the $H^{13}C^{14}N$. The position of seventeen lines out of the total of fifty-six was already published in [8]. Those lines are marked by $^{+}$ in the Tab. 7.1. The rest of the lines are yet to be published.

The position of the absorption line centre was calculated to zero pressure using pressure shift coefficients measured in [9]. As authors did not measure pressure shift coefficients of all of the absorption lines, a non-linear interpolation/extrapolation was used to obtain missing coefficients (these are marked in the Tab. 7.1 by *).

In the uncertainty of each measured line, these effects were considered (as mentioned in [8]): the uncertainty of the pressure shift coefficients and the pressure shift (≈ 10 kHz), the spread of measured absorption lines centre (≈ 5 kHz), the uncertainty of a fitting linear function (≈ 3 kHz), the residual zero offset and background profile (≈ 3 kHz), the residual offsets and drifts in the harmonic detection analogue control (≈ 3 kHz), and the additional safety margin for potential systematic shift effects. The safety margin was increased for the R2 and the R3 absorption lines due to the observed line profile distortion. The safety margin was also increased for the R27-R24 and the P25-P28 lines due to potential non-linear extrapolation error.

The measured absorption lines' centre position was compared [52] with those published in [9]. Both results corresponded at λ =1560 nm, where the wavelength meter in the [9] was referenced. At the wavelengths other than 1560 nm, the difference between data varies. On the other hand, with few exceptions, the difference never gets higher than the uncertainty stated by authors in [9]. We assume that the differences between the data were the reason behind the discrepancies in the calibration using $H^{13}C^{14}N$ absorption cells [7].

The presented measurements of $2\nu_3$ band of $H^{13}C^{14}N$ constitute about fortyfold improvement to data published to date. Hopefully, this could significantly help to accept $H^{13}C^{14}N$ as a suitable spectroscopic medium. Moreover, it would lead to inclusion of $H^{13}C^{14}N$ on the list of *Recommended values of standard frequencies* [3] and *Mise en pratique for the definition of the metre in the SI* [10].

Table 7.1: Centre frequencies of $2\nu_3$ band of $H^{13}C^{14}N$ absorption lines interpolated to zero pressure.

Line	This work f_{ISI} (MHz)	Difference δf (MHz)	Line	This work f_{ISI} (MHz)	Difference δf (MHz)
R27	196299247.932 (40)*	- 0.011	P1	194277572.890 (25)	0.604
R26	196246352.984 (40)*	0.343	P2	194190062.885 (25)*	0.543
R25	196192245.155 (40)*	0.632	P3	194101385.001 (25)*	0.472
R24	196136925.519 (40)*	0.800	P4	194011541.171 (25)$^+$	0.397
R23	196080395.145 (25)$^+$	0.995	P5	193920533.536 (25)$^+$	0.490
R22	196022655.178 (25)*	1.011	P6	193828364.208 (25)*	0.473
R21	195963706.778 (25)	1.124	P7	193735035.335 (25)$^{+*}$	0.438
R20	195903551.125 (25)*	1.069	P8	193640549.115 (25)*	0.358
R19	195842189.486 (25)*	1.012	P9	193544907.760 (25)	0.427
R18	195779623.109 (25)$^+$	1.048	P10	193448113.529 (25)$^+$	0.344
R17	195715853.317 (25)*	0.923	P11	193350168.716 (25)	0.299
R16	195650881.446 (25)*	0.985	P12	193251075.636 (25)*	0.336
R15	195584708.867 (25)	0.810	P13	193150836.645 (25)*	0.373
R14	195517337.014 (25)*	0.881	P14	193049454.131 (25)	0.318
R13	195448767.320 (25)*	0.744	P15	192946930.515 (25)*	0.318
R12	195379001.274 (25)$^+$	0.719	P16	192843268.251 (25)$^+$	0.263
R11	195308040.399 (25)$^{+*}$	0.735	P17	192738469.822 (25)	0.278
R10	195235886.247 (25)	0.575	P18	192632537.753 (25)*	0.240
R9	195162540.395 (25)$^+$	0.640	P19	192525474.593 (25)*	0.258
R8	195088004.481 (25)$^+$	0.584	P20	192417282.929 (25)$^+$	0.189
R7	195012280.156 (25)$^+$	0.536	P21	192307965.380 (25)*	0.127
R6	194935369.109 (25)*	0.493	P22	192197524.596 (25)*	0.034
R5	194857273.056 (25)$^+$	0.561	P23	192085963.269 (25)	0.004
R4	194777993.774 (25)*	0.481	P24	191973284.118 (25)$^+$	- 0.162
R3	194697533.032 (40)$^+$	0.449	P25	191859489.898 (40)*	- 0.370
R2	194615892.657 (40)$^{+*}$	0.422	P26	191744583.389 (40)*	- 0.577
R1	194533074.564 (25)	0.400	P27	191628567.416 (40)*	- 0.971
R0	194449080.484 (25)	0.407	P28	191511444.841 (40)*	- 1.375

$^+$ Absorption lines centres published in [8].

* Absorption lines, for which the pressure shift coefficient was not measured in [9]. The pressure shift coefficient for these lines was obtained by a non-linear interpolation/extrapolation.

8. Conclusion

In this doctoral thesis, I concentrated on the precise measurement of $H^{13}C^{14}N$ $2\nu_3$ band absorption lines position. To reach the objectives, I worked with an external cavity laser that scans the whole $H^{13}C^{14}N$ spectrum (1527 nm - 1565 nm). The laser frequency was measured using the beat note against the optical frequency comb. These two devices' operation principles are described in the Chapter 3.

The linear absorption spectroscopy is a relatively simple method allowing the study of absorption gases. This method is described in section 4.1. In the past, the linear absorption spectroscopy was applied for the $H^{13}C^{14}N$ absorption lines measurement already. In the most recent article [9], authors calculated the position of $H^{13}C^{14}N$ absorption lines with the uncertainty of 1 MHz. They also measured the pressure shift coefficients, permitting them to compare measurements at different gas pressures. In addition, they were able to subtract the pressure shift and to calculate the absorption line position at zero pressure.

The first experiments on the linear absorption spectroscopy were carried out with the Koheras Adjustik E15 laser. As the laser scanning range was only about 1 nm, it enabled me to measure a single absorption line (R2). The laser was frequency-locked to the minimum of the absorption line and kept as such for 8 hours. The achieved fractional frequency stability was in 10^{-8} order. These results were printed in [41].

Further experiments were done with the external cavity laser CTL 1550, that covers the whole absorption spectrum of the $H^{13}C^{14}N$. The position of twenty-six absorption lines [44], with the 2σ standard deviation of the frequency between 40 kHz and 70 kHz was measured. It corresponded to the relative stability of a laser locked to the absorption line minimum of about $9 * 10^{-12}$ at 1 s integration time. The repeatability of the measurement was the issue, as the absolute frequency after relocking to the absorption line minimum was varying in the 1 MHz order.

Moreover, a modulation-free approach was focused on, as that allowed us to measure the whole profile of the absorption line. The troubles with the background in the absorption spectrum were not successfully solved, even though the maximum effort was invested. The polarisation fluctuation was minimised using the Glan-Taylor crystal, and the temperature fluctuation of the absorption cell was decreased by building the temperature-controlling device.

The pressure coefficients were measured (see Tab. 6.1). As only two absorption cells were used, the uncertainty of the coefficients was higher than compared to the [9]. On the other hand, the coefficient trend corresponds well with [9].

The Doppler broadening represents the principal limitation of the linear absorption spectroscopy measurements. The saturation absorption spectroscopy is overcoming the limitation by selectively saturating the absorption gas molecules moving perpendicular to the laser beam, as discussed in the section 4.2. The saturation of $H^{13}C^{14}N$ absorption lines was successfully performed in [35], [37]. On the contrary, no one measured the position of absorption lines or created a table of these absorption lines' centres.

Prior to the saturation absorption experiments, the optimal optical power vs. gas pressure was calculated. The calculation showed two possibilities, either to use the high optical power or the low gas pressure. Given the conditions at the time, it was decided to start with the high optical power approach. The Koheras Adjustik E15 laser seeded

the Koheras Boostik amplifier. Even though the saturation of the R2 absorption line was observed, the results were hardly publishable and inconclusive.

Following saturation spectroscopy experiments involved building the vacuum setup. Its purpose was to refill the absorption cell with sufficiently low $H^{13}C^{14}N$ pressure. It was necessary due to the lack of low-pressure cells on the market. The experiments involved external cavity laser CTL 1550 seeded to the erbium-doped fibre amplifier (EDFA). The experimental configuration Fig. 7.2 led to the observation of the saturated absorption line profile. The repeated scanning of the profile showed the degradation of the S/N ratio as reported in [50].

The issue with the S/N ratio degradation was successfully fixed. As a solution, the S/N ratio degradation was suppressed to the level where the systematic study of the absorption lines was possible. It allowed to use the experimental configuration Fig. 7.4 and to measure the position of fifty-six absorption lines' centre with the precision of 25 kHz. This represents the very first measurement of the $H^{13}C^{14}N$ absorption lines' centre position using the saturation absorption spectroscopy. This result also improves the precision of the prior data on $H^{13}C^{14}N$ [9] of about fortyfold [8]. Besides, this improvement in the precision could lead to the wider application of $H^{13}C^{14}N$, as the reachable accuracy could improve.

The ultimate goal is to is to get included some of the $H^{13}C^{14}N$ lines in the list of *Recommended values of standard frequencies* [3]. To achieve this it is crucial that other experimental groups from all over the world further devote to the study of the saturated absorption data to demonstrate the repeatability of the measurement. To conclude, the following important step would be to improve the precision of the pressure shift coefficient published in [9].

9. Bibliography

[1] Bureau International des Poids et Mesures. Resolution 1 of the 26th CGPM (2018). Online. Available from: https://www.bipm.org/en/committees/cg/cgpm/26-2018/resolution-1. [visited on 22-01-2024].

[2] A. J. Lewis, A. Yacoot, M. J. T. Milton, and A. J. Lancaster. A digital framework for realising the SI—a proposal for the metre. *Metrologia* 59 (4), 044004 (2022). doi: 10.1088/1681-7575/ac7fce.

[3] F. Riehle, P. Gill, F. Arias, and L. Robertsson. The CIPM list of recommended frequency standard values: guidelines and procedures. *Metrologia* 55 (2), 188–200 (2018). doi: 10.1088/1681-7575/aaa302.

[4] T.H. Yoon, J. Ye, J.L. Hall, and J.M. Chartier. Absolute frequency measurement of the iodine-stabilized He-Ne laser At 633 nm. *Applied Physics B* 72 (2), 221-226 (2001). doi: 10.1007/s003400000473.

[5] J. Lazar, J. Hrabina, P. Jedlicka, and O. Cip. Absolute Frequency Shifts Of Iodine Cells For Laser Stabilization. *Metrologia* 46 (5), 450-456 (2009). doi: 10.1088/0026-1394/46/5/008.

[6] T.W. Hänsch, M. D. Levenson, and A. L. Schawlow. Complete Hyperfine Structure Of A Molecular Iodine Line. *Physical Review Letters* 26 (16), 946-949 (1971). doi: 10.1103/PhysRevLett.26.946.

[7] J. Dale, B. Hughes, A. J. Lancaster, A. J. Lewis, A. J. H. Reichold. and M. S. Warden. Multi-channel absolute distance measurement system with sub ppm-accuracy and 20 m range using frequency scanning interferometry and gas absorption cells. *Optics Express* 22 (20), 24869–24893 (2014). doi: 10.1364/OE.22.024869.

[8] J. Hrabina, M. Hosek, S. Rerucha, M. Cizek, Z. Pilat, M. Zucco, J. Lazar, and O. Cip. Absolute frequencies of $H^{13}C^{14}N$ hydrogen cyanide transitions in the 1.5-μm region with the saturated spectroscopy and a sub-kHz scanning laser. *Optics Letters* 47 (21), 5704-5707 (2022). doi: 10.1364/OL.467633.

[9] W. C. Swann, and S. L. Gilbert. Line centers, pressure shift, and pressure broadening of 1530-1560 nm hydrogen cyanide wavelength calibration lines. *Journal of the Optical Society of America B* 22 (8), 1749-1756 (2005). doi: 10.1364/JOSAB.22.001749.

[10] R. Schödel, A. Yacoot, and A. Lewis. The new mise en pratique for the metre - a review of approaches for the practical realization of traceable length metrology from 10^{-11} m to 10^{13} m. *Metrologia* 58 (5), 052002 (2021). doi: 10.1088/1681-7575/ac1456.

[11] The Nobel Prize in Physics 1964, NobelPrize.org, Online. Available from: https://www.nobelprize.org/prizes/physics/1964/summary/. [visited on 20-10-2023].

[12] The Nobel Prize in Physics 2005. NobelPrize.org. Online, Available from: https://www.nobelprize.org/prizes/physics/2005/summary/ [visited on 20-10-2023].

[13] W. Demtröder. *Laser Spectroscopy: Vol. 1: Basic Principles.* 4 edition. Berlin: Springer. 2008. ISBN: 10.1007/978-3-540-73418-5.

[14] W. C. Swann and S. L. Gilbert, *Acetylene* $^{12}C_2H_2$ *absorption reference for* 1510 nm *to* 1540 nm *wavelength calibration - SRM 2517.* Standard Reference Materials. National Institute of Standards and Technology. 2001.

[15] S. L. Gilbert, W. C. Swann, *Carbon monoxide absorption references for* 1560 nm *to* 1630 nm *wavelength calibration - SRM 2514.* Standard Reference Materials. National Institute of Standards and Technology. 2002.

[16] J. Hrabina, M. Hola, J. Lazar, M. Sarbort, and O. Cip. Spectral Properties of Saturation Pressure Filled Iodine Absorption Cells. *Applied Optics* 53 (31), 839-842 (2014). doi: 10.1007/978-3-642-36359-7_153.

[17] J. Hrabina, O. Acef, F. du Burck, N. Chiodo, Y. Candela, M. Sarbort, M. Hola, and J. Lazar. Comparison of Molecular Iodine Spectral Properties at 514.7 and 532 nm Wavelengths. *Measurement Science Review* 14(4), 213-218 (2014). doi: 10.2478/msr-2014-0029.

[18] S. Schilt, L. Thevenaz, and P. Robert. Wavelength modulation spectroscopy: combined frequency and intensity laser modulation. *Applied Optics* 42 (33), 6728-6738 (2003). doi: 10.1364/AO.42.006728.

[19] Y. Du, Z. Peng, and Y. Ding. Wavelength modulation spectroscopy for recovering absolute absorbance. *Optics Express* 26(7), 9263-9272 (2018). doi: 10.1364/OE.26.009263.

[20] F. Bayer-Helmes, and J. Helmcke. *Modulation broadening of spectral profiles.* PTB-Me-17, PTB-Bericht. 1977.

[21] M. Weel, and A. Kumarakrishnan. Laser-frequency stabilization using a lock-in amplifier. *Canadian Journal of Physics* 80(12), 1449-1458 (2002). doi: 10.1139/p02-084.

[22] W. Demtröder. *Laser Spectroscopy: Vol. 2: Experimental Techniques.* 4 edition Berlin: Springer. 2008. ISBN: 978-3-540-74952-3

[23] O. Firstenberg, M. Shuker, R. Pugatch, D. R. Fredkin, N. Davidson, and A. Ron. Theory of thermal motion in electromagnetically induced transparency: Effects of diffusion, Doppler broadening, and Dicke and Ramsey narrowing. *Physical Review A* 77 (8), 043830 (2008). doi: 10.1103/PhysRevA.77.043830.

[24] A. Lesundak, T. M. Pham, M. Cizek, O. Obsil, L. Slodicka, O. Cip. Optical frequency analysis on dark state of a single trapped ion. *Optics Express* 28(9), 13091-13103 (2020). doi: 10.1364/OE.389411.

[25] A. D. Ludlow, M. M. Boyd, J. Ye, E. Peik, P.O. Schmidt. Optical atomic clocks. *Reviews of Modern Physics* 87(2), 637-701 (2015). doi: 10.1103/RevModPhys.87.637.

[26] H. Sasada, and K. Yamada. Calibration lines of HCN in the 1.5 μm region. *Applied Optics* 29 (24), 3535-3547 (1990). doi: 10.1364/AO.29.003535.

[27] M. Schneider, K. M. Evenson, M. D. Vanek, D. A. Jennings, and J. S. Wells. Heterodyne frequency measurements of $^{12}C^{16}O$ laser transitions. *Journal of Molecular Spectroscopy* 135 (2), 197-206 (1989). doi: 10.1016/0022-2852(89)90150-1.

[28] A. M. Smith, S. L. Coy, W. Klemperer, and K. K. Lehmann. Fourier transform spectra of overtone bands of HCN from 5400 to 15100 cm^{-1}. *Journal of Molecular Spectroscopy* 134 (1), 134-153 (1989). doi: 10.1016/0022-2852(89)90136-7.

[29] S.L. Gilbert, W. C. Swann, and C. M. Wang. Hydrogen cyanide $H^{13}C^{14}N$ absorption reference for 1530-1560 nm wavelength calibration - SRM 2519. *Standard Reference Materials*. National Institute of Standards and Technology. 1998.

[30] K. L. Corwin, I. Thomann, T. Dennis, R. W. Fox, W. Swann, E. A. Curtis, C. W. Oates, G. Wilpers, A. Bartels, S. L. Gilbert, L. Hollberg, N. R. Newbury, S. A. Diddams, J. W. Nicholson, and M. F. Yan. Absolute frequency measurements with a stabilized near-infrared optical frequency comb from a Cr:forsterite laser. *Optics Letters* 29 (4), 397–399 (2004). doi: 10.1364/ol.29.000397

[31] K. Nakagawa, M. de Labachelerie, Y. Awaji, and M. Kourogi. Accurate optical frequency atlas of the 1.5-μm bands of acetylene. *Journal of the Optical Society of America B* 13 (12), 2708–2714 (1996). doi: 10.1364/JOSAB.13.002708.

[32] A. B. Mateo, and Z. W. Barber. Precision and accuracy testing of FMCW ladar-based length metrology. *Applied Optics* 54 (19), 6019-6024 (2015). doi: 10.1364/AO.54.006019.

[33] X. Fan, J. Jiang, X. Zhang, K. Liu, S. Wang, Y. Yang, F. Sun, J. Zhang, C. Guo, J. Shen, S. Wu, and T. Liu. Self-marked HCN gas based FBG demodulation in thermal cycling process for aerospace environment. *Optics Express* 26 (18), 22944-22953 (2018). doi: 10.1364/OE.26.022944.

[34] X. Zhang, Y. Li, H. Hu, J. Jiang, K. Liu, X. Fan, M. Feng and T. Liu. Recovered HCN absorption spectrum-based FBG demodulation method covering the whole C-band for temperature changing environment. *IEEE Access* 8, 15039-15046 (2020). doi: 10.1109/ACCESS.2020.2966084.

[35] M. D. Labachelerie, K. Nakagawa, Y. Awaji, and M. Ohtsu. High-frequency-stability laser at 1.5 μm using Doppler-free molecular lines. *Optics Letters* 20 (6), 572–574 (1995). doi: 10.1364/ol.20.000572.

[36] Y. Awaji, K. Nakagawa, M. de Labachelerie, M. Ohtsu, and H. Sasada. Optical frequency measurement of the $H^{12}C^{14}N$ Lamb-dip-stabilized 1.5 μm diode laser. *Optics Letters* 20 (19), 2024–2026 (1995). doi: 10.1364/ol.20.002024.

[37] J. Henningsen, J. Hald, and J. C. Peterson. Saturated absorption in acetylene and hydrogen cyanide in hollow-core photonic bandgap fibers. *Optics Express* 13 (26), 10475-10482 (2005). doi: 10.1364/OPEX.13.010475.

[38] M. J. D. Low, N. Ramasubramanian, P. Ramamurthy, A. V. Deo. Infrared spectrum, surface reaction, and polymerization of adsorbed hydrogen cyanide on

porous glass. *The Journal of Physical Chemistry* 72(7), 2371-2378 (1968). doi: 10.1021/j100853a016.

[39] K. Ruxton, A.L. Chakraborty, W. Johnstone, M. Lengden, G. Stewart, and K. Duffin. Tunable diode laser spectroscopy with wavelength modulation: Elimination of residual amplitude modulation in a phasor decomposition approach. *Sensors and Actuators B: Chemical* 150(1), 367-375 (2010). doi: 10.1016/j.snb.2010.06.058.

[40] M. Cızek, V. Hucl, J. Hrabina, R. Smıd, B. Mikel, J. Lazar, O. Cıp. Two-stage system based on a software-defined radio for stabilizing of optical frequency combs in long-term experiments. *Sensors* 14 (1), 1757-1770 (2014). doi: 10.3390/s140101757.

[41] M. Hosek, S. Rerucha, L. Pravdova, M. Cizek, J. Hrabina, and O. Cip. Investigating the use of the hydrogen cyanide (HCN) as an absorption media for laser spectroscopy. *Proceedings Volume 10976, 21st Czech-Polish-Slovak Optical Conference on Wave and Quantum Aspects of Contemporary Optics*. 2018. doi: 10.1117/12.2517761.

[42] M. Cizek, L. Pravdova, T. Minh Pham, A. Lesundak, J. Hrabina, J. Lazar, T. Pronebner, E. Aeikens, J. Premper, O. Havlis, R. Velc, V. Smotlacha, L. Altmannova, T. Schumm, J. Vojtech, A. Niessner, and O. Cip. Coherent fibre link for synchronization of delocalized atomic clocks. *Optics Express* 30 (4), 5450-5464 (2022). doi: 10.1364/OE.447498.

[43] W. Riley, and D. Howe, *Handbook of Frequency Stability Analysis*. Special Publication. National Institute of Standards and Technology. 2008.

[44] M. Hosek, S. Rerucha, J. Hrabina, M. Cizek, and O. Cip. Measurement of the Hydrogen Cyanide Absorption Lines' Centers with the Potential for Mise en Pratique. *2021 Joint Conference of the European Frequency and Time Forum and IEEE International Frequency Control Symposium (EFTF/IFCS)*. 2021. doi: 10.1109/EFTF/IFCS52194.2021.9604261.

[45] M. Hosek, S. Rerucha, J. Hrabina, M. Cizek, L. Pravdova, and O. Cip. High-precision measurement of the center frequencies of the hydrogen cyanide (HCN) hyperfine transitions in the 1.5 μm wavelength band. *Proceedings Volume 12502, 22nd Polish-Slovak-Czech Optical Conference on Wave and Quantum Aspects of Contemporary Optics*. 2022. doi: 10.1117/12.2664209.

[46] W.C. Swann, and S.L. Gilbert. Accuracy limits for simple molecular absorption based wavelength references. *Technical Digest: Symposium on Optical Fiber Measurements*, 15-18 (2004). doi: 10.1109/SOFM.2004.183465.

[47] O. Cip, *Frequency stabilization of laser diodes and high precision laser interferometry*. Ph.D. thesis. Brno University of Technology, Faculty of Electrical Engineering and Computer Sciences. 2001.

[48] P.W. Hastings, M. K. Osborn, C. M. Sadowski, and I. W. M. Smith. Vibrational relaxation of HCN(002). *The Journal Of Chemical Physics* 78 (6), 3893-3898 (1983). doi: 10.1063/1.445111.

[49] R.J. Barber, G. J. Harris, and J. Tennyson. 2002. Temperature dependent partition functions and equilibrium constant for HCN and HNC. *The Journal Of Chemical Physics* 117 (24), 11239-11243 (2002). doi: 10.1063/1.1521131.

[50] J. Hrabina, M. Hosek, S. Rerucha, L. Pravdova, J. Lazar, O. Cip, and Z. Pilat. Saturated Spectroscopy of HCN. 2021 Joint Conference of the European Frequency and Time Forum and IEEE International Frequency Control Symposium (EFTF/IFCS). 2021. doi: 10.1109/EFTF/IFCS52194.2021.9604272.

[51] O. Cip, A. Lesundak, T. M. Pham, V. Hucl, M. Cizek, S. Rerucha, J. Hrabina, J. Lazar, P. Obsil, R. Filip, and L. Slodicka. The compact setup for laser cooling and high-resolution spectroscopy with cold $^{40}Ca^{+}$ ions. *2018 European Frequency and Time Forum (EFTF)*. 2018. doi: 10.1109/EFTF.2018.8409077.

[52] M. Hosek, J. Hrabina, S. Rerucha, M. Cizek, L. Pravdova, and O. Cip. Saturation Spectroscopy of $H^{13}C^{14}N$ Absorption Lines. *2023 Joint Conference of the European Frequency and Time Forum and IEEE International Frequency Control Symposium (EFTF/IFCS)*. 2023. doi: 10.1109/EFTF/IFCS57587.2023.10272040.